Article

Cell Reports

Aerobic Glycolysis Is Essential for Normal Rod Function and Controls Secondary Cone Death in Retinitis Pigmentosa

Graphical Abstract

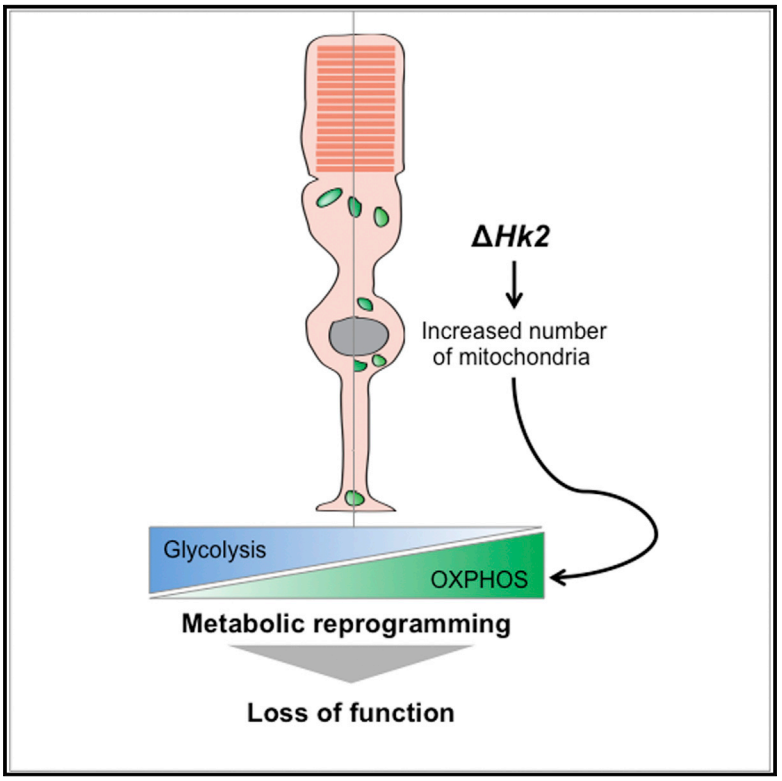

Authors

Lolita Petit, Shan Ma, Joris Cipi, Shun-Yun Cheng, Marina Zieger, Nissim Hay, Claudio Punzo

Correspondence

claudio.punzo@umassmed.edu

In Brief

Photoreceptors are terminal differentiated neurons using aerobic glycolysis to meet their metabolic needs. Using a hexokinase-2 conditional mouse, Petit et al. show that photoreceptors do not need hexokinase-2 for survival but rather for function and adaptation to metabolic stress.

Highlights

- Loss of HK2 in rod PRs inhibits aerobic glycolysis
- Inhibition of aerobic glycolysis impairs only rod function, not rod survival
- Increased OXPHOS largely compensates the inhibition of aerobic glycolysis
- HK2 confers a survival advantage in cones under metabolic stress conditions

Petit et al., 2018, Cell Reports *23*, 2629–2642
May 29, 2018
https://doi.org/10.1016/j.celrep.2018.04.111

CellPress

Cell Reports
Article

Aerobic Glycolysis Is Essential for Normal Rod Function and Controls Secondary Cone Death in Retinitis Pigmentosa

Lolita Petit,[1] Shan Ma,[1] Joris Cipi,[1] Shun-Yun Cheng,[1] Marina Zieger,[2] Nissim Hay,[3] and Claudio Punzo[1,4,*]
[1]Department of Ophthalmology and Gene Therapy Center, University of Massachusetts Medical School, Worcester, MA, USA
[2]Division of Pulmonary Medicine, Department of Pediatrics, University of Massachusetts Medical School, Worcester, MA, USA
[3]Department of Biochemistry and Molecular Genetics, College of Medicine, University of Illinois at Chicago, Chicago, IL, USA
[4]Lead Contact
*Correspondence: claudio.punzo@umassmed.edu
https://doi.org/10.1016/j.celrep.2018.04.111

SUMMARY

Aerobic glycolysis accounts for ~80%–90% of glucose used by adult photoreceptors (PRs); yet, the importance of aerobic glycolysis for PR function or survival remains unclear. Here, we further established the role of aerobic glycolysis in murine rod and cone PRs. We show that loss of hexokinase-2 (HK2), a key aerobic glycolysis enzyme, does not affect PR survival or structure but is required for normal rod function. Rods with HK2 loss increase their mitochondrial number, suggesting an adaptation to the inhibition of aerobic glycolysis. In contrast, cones adapt without increased mitochondrial number but require HK2 to adapt to metabolic stress conditions such as those encountered in retinitis pigmentosa, where the loss of rods causes a nutrient shortage in cones. The data support a model where aerobic glycolysis in PRs is not a necessity but rather a metabolic choice that maximizes PR function and adaptability to nutrient stress conditions.

INTRODUCTION

Rod and cone photoreceptors (PRs) are the neurons ensuring light detection in the retina. Although terminally differentiated and non-proliferative, PRs are among the most metabolically active cells of the body (Ames, 2000). In the dark, they consume considerable ATP amounts to activate ion pumps in their plasma membrane that maintain membrane excitability. In the light, they use energy to support visual signal transduction (Okawa et al., 2008). While maintaining homeostasis, PRs have very high biosynthetic requirements. PRs replace daily 10% of their outer segment (OS), a protein and lipid rich organelle, that is lost to phagocytosis by the retinal pigment epithelium (RPE) (LaVail, 1976). Yet, we have to fully understand how PRs regulate metabolic pathways to meet both their energetic and anabolic demands, and how this affects PR function and survival. A better understanding of the regulation of PR metabolism is important to determine why PRs die due to energy stress in a number of human blinding diseases (Aït-Ali et al., 2015; Joyal et al., 2016; Punzo et al., 2009; Zhang et al., 2016).

Neurons depend on glucose as their main energy source (Mergenthaler et al., 2013). However, PRs particularity is to consume glucose in excess of that used for oxidative phosphorylation (OXPHOS) despite sufficient oxygen to metabolize glucose completely. Consequently, they convert most of their glucose to lactate (Chinchore et al., 2017; Cohen and Noell, 1960; Narayan et al., 2017; Wang et al., 1997; Winkler, 1981). This process, referred to as aerobic glycolysis, is a hallmark of cancer cells, where it supports unrestrained proliferation (Vander Heiden et al., 2009). In PRs, aerobic glycolysis is thought to promote the biomass necessary for OS renewal (Chinchore et al., 2017). However, the balance between aerobic glycolysis and OXPHOS in PRs *in vivo* is unknown and the importance of aerobic glycolysis for survival and function of PRs has not been evaluated. Moreover, cones and rods have different energy requirements (Hoang et al., 2002; Narayan et al., 2017; Nikonov et al., 2008; Okawa et al., 2008; Perkins et al., 2003; Rueda et al., 2016). Whether aerobic glycolysis has the same role in both PR subtypes remains to be investigated.

Here, the importance of aerobic glycolysis in PRs was investigated by specifically inhibiting in cones and rods a gatekeeper of aerobic glycolysis: hexokinase (HK) 2 (Gershon et al., 2013; Roberts and Miyamoto, 2015; Wolf et al., 2011). HK catalyzes the first critical step of glycolysis: the ATP-dependent conversion of glucose to glucose-6-phosphate (G-6-P). Among the four mammalian HK isoenzymes, HK1 is the most ubiquitously expressed HK (Wilson, 2003). In contrast, HK2 is absent from most adult tissues (Wilson, 2003) but is overexpressed in most cancer cells as part of the general strategy to reprogram cell metabolism toward aerobic glycolysis (Gershon et al., 2013; Mathupala et al., 1997, 2006; Patra et al., 2013; Rempel et al., 1996; Roberts and Miyamoto, 2015; Wolf et al., 2011). The preferential mitochondrial localization of both HK1 and HK2 provides direct access to ATP generated by OXPHOS to promote rapid glucose phosphorylation (Arora and Pedersen, 1988; Mathupala et al., 2006). It also generates an ADP/ATP recycling mechanism to maintain high OXPHOS rates. AKT directly modulates mitochondrial HK2 (Roberts et al., 2013), which may allow tumor cells to dynamically adapt glycolysis depending on the metabolic state (Mergenthaler et al., 2012; Roberts and Miyamoto, 2015). Given that PRs express high levels of HK2 (Aït-Ali et al., 2015; Rajala

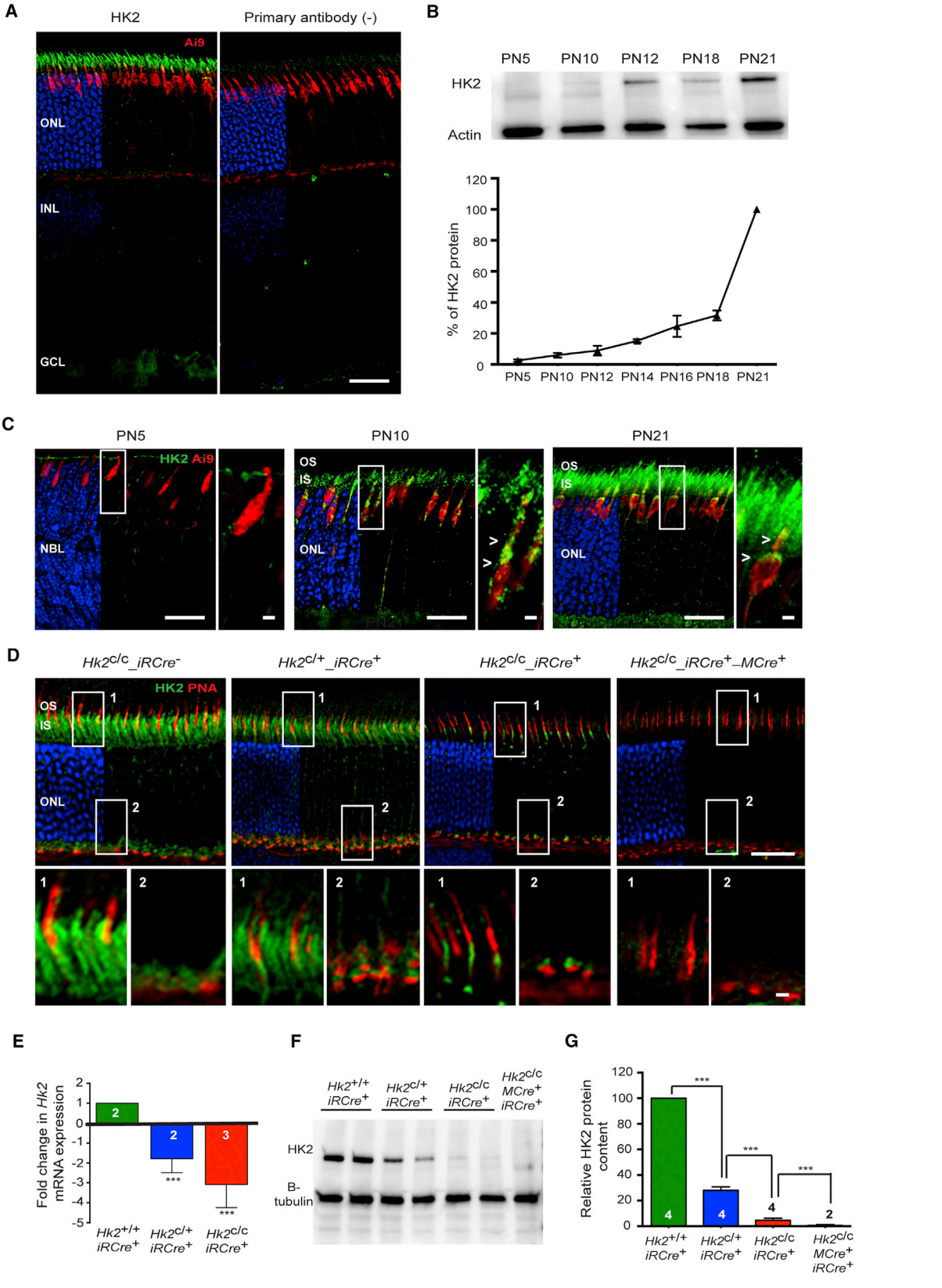

(legend on next page)

et al., 2013; Reidel et al., 2011; Rueda et al., 2016), we hypothesized that HK2 couples aerobic glycolysis to PR survival and/or function. Here, we show that HK2 promotes aerobic glycolysis in PRs, and loss of HK2-mediated aerobic glycolysis correlates with increased OXPHOS. This reprogramming has no impact on PR survival rather it impairs rod function. Moreover, HK2 is required to help cones to survive under metabolic stress.

RESULTS

HK2 Is Expressed at Comparable Levels in Rods and Cones

To elucidate the role of *Hk2* and aerobic glycolysis in PRs, we first confirmed that HK2 is present in both rods and cones and that PR-specific loss of function is achieved. As expected (Aït-Ali et al., 2015; Rajala et al., 2013; Reidel et al., 2011; Rueda et al., 2016), HK2 expression was PR-enriched and increased during the postnatal maturation of PRs (Figures 1A–1C). Western blot analysis confirmed the specificity of the HK2 antibody (Figure S1A). Using the *Ai9_MCre*$^{+}$ line, which conditionally expresses the fluorescent tdTomato protein in cones, we confirmed that *Hk2* is also expressed in cones (Figures 1C and S1B). Cone expression was further validated on retinal flatmounts of *Nrl*$^{-/-}$ mice, which have no rods due to a developmental reprogramming of rods into cones (Figure S1B). Immunohistochemistry (IHC) showed that HK2 was localized to the inner segment (IS) and the synaptic terminal of PRs (Figure 1D). In cones, HK2 was also localized within the perinuclear region (Figures 1C and 1D).

Loss of HK2 function in rods or cones was achieved by crossing the *Hk2* conditional mouse (*Hk2*$^{c/c}$) to the rod-specific *iRCre* line or the cone-specific *MCre* line, respectively. Cell-type specificity and developmental expression analyses of both *Cre* lines showed that at least 89% and 100% of rods and cones, respectively, express CRE recombinase (Figures S1D and S1H), with *Cre* expression becoming evident by post-natal day (PN) 5–7 (Figures S1E and S1F). HK2 loss was confirmed at the RNA and protein level and by IHC (Figures 1D–1G and S1I). Mice heterozygous for *Hk2* in rods (*Hk2*$^{c/+}$*_iRCre*$^{+}$) displayed a 50%–70% decrease in HK2 RNA and protein levels when compared to wild-type mice (Figures 1D–1G). To confirm the loss of HK2 in cones, we generated mice with simultaneous *Hk2* deletion in rods and cones (*Hk2*$^{c/c}$*_iRCre*$^{+}$*_MCre*$^{+}$*).* These mice had no residual HK2 protein in the retina (Figures 1D, 1F, and 1G). The data show that both rods and cones express HK2, and one allele is not sufficient to achieve normal expression. Additionally, the remainder of HK2 protein in *Hk2*$^{c/c}$*_iRCre*$^{+}$ mice and the complete absence of the protein after *Hk2* deletion in rods and cones suggests that cones and rods express comparable levels of HK2.

HK2 Loss Inhibits Aerobic Glycolysis in Rods

Hk2 knockout in cancer cells leads to loss of aerobic glycolysis (Wolf et al., 2011). To determine if HK2 loss also inhibits aerobic glycolysis in PRs, critical glycolysis enzymes and extracellular lactate production were evaluated in 1-month-old *Hk2*$^{c/c}$*_iRCre*$^{-}$, *Hk2*$^{c/+}$*_iRCre*$^{+}$, and *Hk2*$^{c/c}$*_iRCre*$^{+}$ mice (Figures 2 and S2). Lactate dehydrogenase (LDH) mediates the bidirectional conversion between pyruvate and lactate and constitutes an important switch between aerobic glycolysis and OXPHOS (Valvona et al., 2016). LDH is a tetrameric enzyme composed of LDHA and LDHB subunits, which have different substrate and product affinities. Consequently, the relative proportion of LDHA and LDHB within the LDH tetramer changes the reaction rate and thereby the steady-state levels in cells. LDHA, which has a higher affinity for pyruvate, is generally associated with high rates of aerobic glycolysis (Read et al., 2001; Valvona et al., 2016). Because of that, LDHA is expressed at high levels in PRs (Casson et al., 2016; Chinchore et al., 2017; Rueda et al., 2016). We found reduced expression of LDHA after partial or total ablation of HK2 in rods (Figures 2A, 2B, and S2). In contrast, the low levels of LDHB remained unchanged (Figures 2A, 2B, and S2). Expression of pyruvate kinase muscle isozyme M2 (PKM2), another enzyme promoting anabolism (Iqbal et al., 2013, 2014), was also decreased in *Hk2*$^{c/c}$*_iRCre*$^{+}$ retinas, but no change was seen in *Hk2*$^{c/+}$*_iRCre*$^{+}$ mice (Figures 2A, 2B, and S2). Previous work established an essential role for LDHA and PKM2 in supporting lactate production by rods (LDHA and PKM2 conditional knockout decreased lactate secretion by ~57% and ~14% per Cre^{+} rods, respectively). Similarly, we observed a significant reduction in extracellular lactate in both *Hk2*$^{c/c}$*_iRCre*$^{+}$ and *Hk2*$^{c/+}$*_iRCre*$^{+}$ retinas (loss of ~39% of extracellular lactate per Cre^{+} rods, Figure 2C). Inhibiting HK2-mediated aerobic glycolysis also resulted in a significant reduction in NAPDH in *Hk2*$^{c/c}$*_iRCre*$^{+}$*,* but not *Hk2*$^{c/+}$*_ iRCre*$^{+}$ retinas (Figure 2C). The equivalent experiment with HK2 loss in cones was not carried out, as cones account only for 3% of PRs making it difficult to detect changes in total retinal extracts. The data indicate that at least in rods, HK2 loss inhibits aerobic glycolysis.

Minimal Cell Death in HK2-Deficient PRs

To study the effect of HK2-mediated aerobic glycolysis in PRs, we performed funduscopy and histological analyses over a

Figure 1. HK2 Expression in Cones and Rods

(A) HK2 expression (green) by IHC in adult *Ai9_MCre*$^{+}$ retinas (red: tdTomato in *Ai9_MCre*$^{+}$ mice). Right: no primary antibody. Blue: DAPI, removed from 60% of panels to visualize red and green signals.

(B) Developmental expression and quantification of HK2 by western blot with retinal extracts (loading control: actin; n = 3; levels expressed as % of PN21 levels).

(C) Developmental expression of HK2 by IHC at ages indicated with same labeling as in (A). Higher magnification of boxed area is shown to the right of each panel (arrowheads: HK2 in cones).

(D) HK2 expression (green) in retinas of genotypes indicated (red, PNA detecting cones; blue, DAPI, removed from 60% of panels to visualize red and green signals; age: 1 month). Higher magnifications of areas 1 and 2 are shown below each panel.

(E) Relative levels of retinal *Hk2* RNA after conditional *Hk2* deletion in rods (GAPDH: reference; age: 1 month).

(F and G) Western blot (F) and quantification (G) of retinal HK2 protein levels in genotypes indicated (levels expressed as % of wild-type; age: 1 month).

Errors bars ± SD; numbers in bars, number of retinas analyzed; OS, outer segment; IS, inner segment; ONL, outer nuclear layer; INL, inner nuclear layer; GCL, ganglion cell layer. Scale bars, 25 μm (long one), 5 μm (short one).

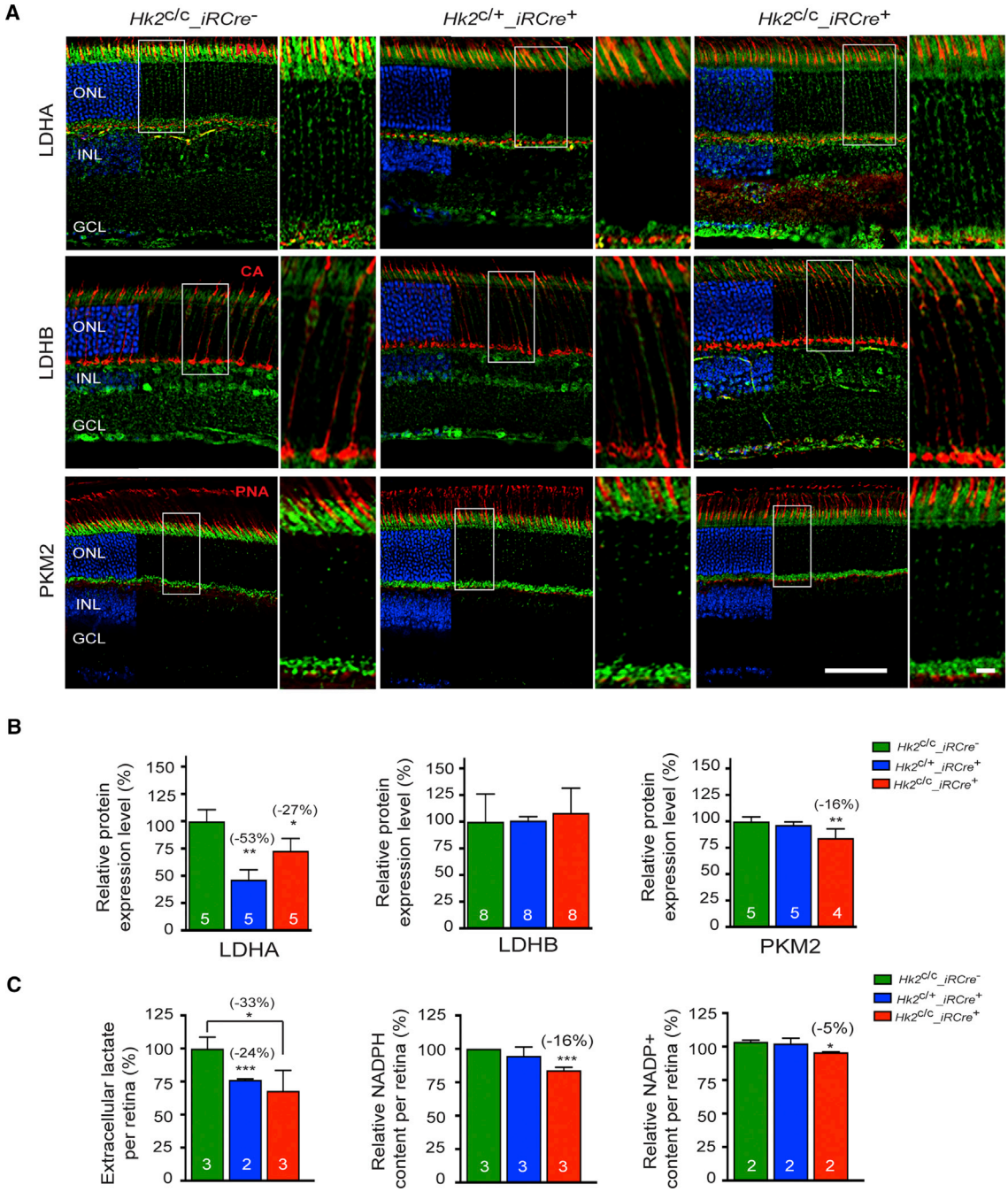

Figure 2. Changes in Aerobic Glycolysis upon HK2 Loss in Rods

(A–C) One-month-old mice of genotypes indicated in panels.

(A) IHC on retinal sections for proteins indicated to the left of each panel (green signal). Cones (red signal) were detected by PNA or with an anti-cone arrestin (CA) antibody (blue: DAPI, removed from 60% of panels to visualize red and green signals; higher magnification of boxed area is shown to the right of each panel).

(B) Quantitative western-blot analysis with retinal extracts for proteins indicated (levels expressed as % of wild-type).

(C) Quantification of lactate, NADPH and $NADP^+$ from freshly dissected retinas.

Errors bars ± SD; numbers in bars, number of biological samples (each consisting of 2 retinas from one mouse); ONL, outer nuclear layer; INL, inner nuclear layer; GCL, ganglion cell layer. Scale bars: 85 μm (long one), 10 μm (short one).

12-month period on mice with *Hk2* loss in rods (Figures 3A–3D and S3) or cones (Figures 3E–3G). Surprisingly, we found no evidence of PR cell death at any age tested in both $Hk2^{c/c}$_$iRCre^{+}$ and $Hk2^{c/c}$_$MCre^{+}$ lines. PR numbers (Figures 3B and 3F), outer nuclear layer (ONL) thickness (Figure 3C), OS length and structure (Figures S3A–S3C) were similar to control mice. Expression of PR-specific markers was also unaffected (Figures 3D, 3G, and S3D), indicating that rods and cones survive under conditions of aerobic glycolysis deficiency.

Aerobic Glycolysis Deficiency Alters Rod, but Not Cone, Function

The long-term viability of HK2-deficient PRs allowed us to test how aerobic glycolysis supports PR function. Electroretinography (ERG) at 1 month showed an ~30% reduction in the rod scotopic a- and b-waves amplitudes in $Hk2^{c/c}$_$iRCre^{+}$ mice when compared to $Hk2^{c/c}$_$iRCre^{-}$ and $Hk2^{c/+}$_$iRCre^{+}$ mice (Figures 4A–4E and 4H). We extended these results by comparing the leading edges of the scotopic a-wave responses of $Hk2^{c/c}$_$iRCre^{-}$, $Hk2^{c/+}$_$iRCre^{+}$, and $Hk2^{c/c}$_$iRCre^{+}$ mice after normalization (Hood and Birch, 1996-1997) (Figure 4E). The overlap of $Hk2^{c/c}$_$iRCre^{-}$ and $Hk2^{c/+}$_$iRCre^{+}$ leading edges indicates that $Hk2^{c/+}$ rods keep normal phototransduction kinetics. In $Hk2^{c/c}$_$iRCre^{+}$ mice, the a-wave response was reduced compared to $Hk2^{c/c}$_$iRCre^{-}$ mice; yet this reduction remained constant at all times (Figure 4E), indicating that the phototransduction cascade is not slowed. The amplitude reduction likely reflects a perturbation of the dark current and/or glutamate vesicle release. Rod responses were also delayed in implicit time (Figures 4F and 4G). Interestingly, the reduction of the rod responses remained stable for up to 18 months (Figure 4H), suggesting that inhibition of aerobic glycolysis stably impairs rod function. HK2 loss in rods did not affect cone function (Figure 4I). Unlike rods, HK2 loss in cones had no effect on PR function (Figures 4J and 4K). The results further confirm metabolic differences between cones and rods and suggest that unlike rods, cones do not depend on aerobic glycolysis or that they are better able to adapt to its inhibition.

Inhibition of HK2-Mediated Aerobic Glycolysis Rebalances PR Metabolism in Rods

To understand how the inhibition of aerobic glycolysis impairs rod function, we evaluated changes in selected glycolytic pathways. PRs in culture can produce ATP via OXPHOS when aerobic glycolysis in inhibited (Chinchore et al., 2017). PR mitochondria also provide an alternative metabolic pathway for NADPH generation in isolated mouse rods under transient glucose shortage (Adler et al., 2014). We therefore assessed mitochondrial changes in HK2-deficient PRs. The mitochondrial marker voltage-dependent anion channel (VDAC) was found to be upregulated in $Hk2^{c/c}$_$iRCre^{+}$ retinas at 1 month of age when compared to control mice (Figures 5A–5C). In $Hk2^{c/+}$_$iRCre^{+}$ and control mice, VDAC staining was mainly localized to the PR IS. While a similar staining was observed in $Hk2^{c/c}$_$iRCre^{+}$ retinas, large $VDAC^{+}$ dots were also observed in the ONL with a tendency of these dots to concentrate toward the outer limiting membrane (OLM) (Figures 5A, 5C, and 5F). Similar large dots were observed with HK1 staining (Figures 5D–5F and S4A). $VDAC^{+}$ or $HK1^{+}$ large dots did not overlap with the Muller glia marker glutamine synthase (Figures 5C, 5D, and S4A) or with the cone marker cone arrestin (Figure 5E), indicating that mitochondrial changes occurred in rods. The increased VDAC expression in $Hk2^{c/c}$_$iRCre^{+}$ retinas was also associated with a marked upregulation of mitochondrial OXPHOS proteins (Figures 5G and S2B). Transmission electron microscopy confirmed a higher number of mitochondria in HK2-deficient rods compared with controls (Figures 5H, 5I, and S3E–S3G). These mitochondria were in the distal perinuclear area of the rod somas (Figures 5H, S3E, and S3F), a distribution observed in cone PRs only or in avascular retinas. The number and size of perinuclear rod mitochondria in $Hk2^{c/c}$_$iRCre^{+}$ mice increased with age (Figures 5H and S3E).

To determine if the increase in mitochondria number associated with HK2 depletion was due to reduced glucose uptake, retinal explants were cultured in the presence of the fluorescent D-glucose analog 2-NDGB (Figures S5Aand S5B). Fluorescence intensity was decreased when 2-NBDG was inhibited by addition of D-glucose to the media. Interestingly, whereas a slight decrease was observed in $Hk2^{c/+}$_$iRCre^{+}$ retinas compared to controls, $Hk2^{c/c}$_$iRCre^{+}$ retinas showed no difference in glucose uptake when compared to controls. This maintenance in glucose uptake was associated with an upregulation of HK1 and GLUT1 at 1 and 12 months (Figures S4A, S5C, and S5D). In $Hk2^{c/+}$_$iRCre^{+}$ retinas, no significant change in the expression of HK1 and GLUT1 were observed in total retinal extracts (Figure S5C), despite an increase in the number of $HK1^{+}$ dots in the ONL (Figure 5F). We also observed a progressive decline in HK2 expression (Figure S4) and a compensatory upregulation of HK1 in normal rods with age (Figure S4). Thus, although glucose flux was not directly evaluated, the downregulation of enzymes critical for aerobic glycolysis along with decreased lactate levels and an increase in mitochondrial number suggest that the decrease in HK2-meditaed aerobic glycolysis is coupled to elevated OXPHOS. The absence of mitochondrial biogenesis in $Hk2^{c/+}$_$iRCre^{+}$ mice may indicate that rods engage in compensatory mechanisms to maintain a relatively high glycolytic flux that results in a decrease in lactate production with no change in PKM2, and NADPH synthesis. Therefore, increased OXPHOS largely compensates for aerobic glycolysis deficiency in rods.

In cones, only HK1, but not VDAC staining nor mitochondria number, increased upon HK2 loss, possibly reflecting the higher basal OXPHOS capacity of cones compared to rods (Perkins et al., 2003) (Figure S5E).

PRs may use lactate to fuel oxidative metabolism (Pellerin and Magistretti, 1994; Poitry-Yamate et al., 1995). Rods are the main producers of lactate in the retina (Chinchore et al., 2017; Hurley et al., 2015), thus, we considered the possibility that cones can use rod-derived lactate as an alternative fuel to compensate for glycolysis reduction. We performed ERG analyses on mice with simultaneous *Hk2* loss in rods and cones. Remarkably, cone responses were reduced in $Hk2^{c/c}$_$iRCre^{+}$_$MCre^{+}$ mice compared to $Hk2^{c/c}$_$iRCre^{+}$ littermates (Figure 6A), suggesting that when aerobic glycolysis is affected, cones rely on lactate produced by rods. Accordingly, we observed an increase of LDHB in cones of $Hk2^{c/c}$_ $iRCre^{+}$_$MCre^{+}$ mice when compared to $Hk2^{c/c}$_ $iRCre^{+}$_$MCre^{-}$ mice at 2 months (Figure 6B), while

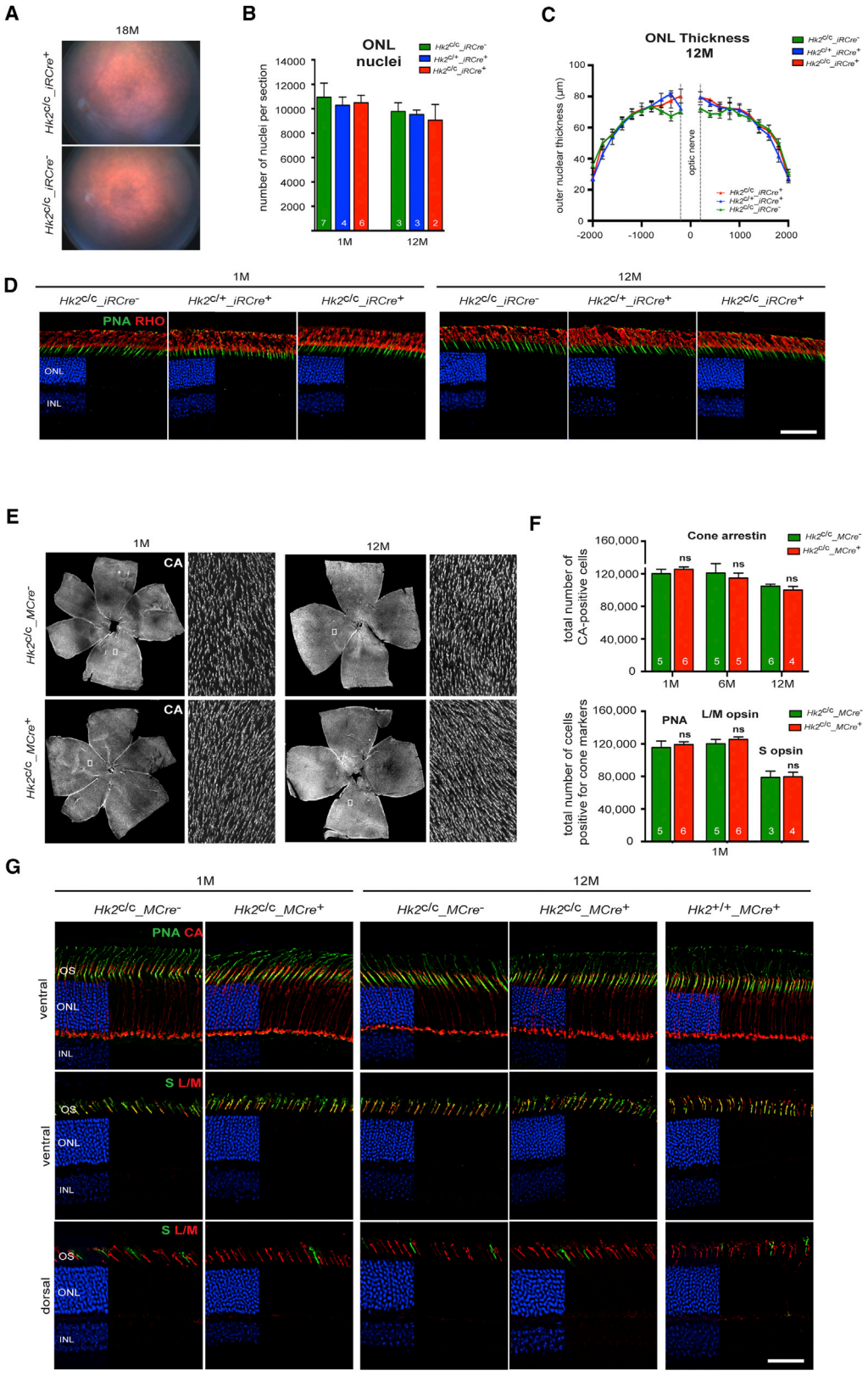

(legend on next page)

there was no change in LDHB expression in *Hk2*$^{c/c}$*_MCre*$^{+}$ mice compared to *Hk2*$^{c/c}$*_MCre*$^{-}$ mice at 1 (Figure 6B) or 12 months (data not shown). Thus, cones adapt to loss of *Hk2* by taking up lactate produced by rods.

Cones under Metabolic Stress Require HK2 to Survive

The balance between aerobic glycolysis and OXPHOS may be altered during disease or conditions of severe metabolic perturbations. To investigate the role of aerobic glycolysis during retinal degeneration, we crossed the *Hk2_MCre*$^{+}$ line with the *retinal degeneration 1* (*rd1*) mouse model of retinitis pigmentosa (RP). In RP, cone death always follows rod death. Accumulative evidence suggests that cones die in RP due to glucose deprivation. We showed that cones upregulate several metabolic genes at the onset of cone death including hypoxia-induced factor 1 (HIF-1a), GLUT1, PKM2 and HK2 (Punzo et al., 2009; Venkatesh et al., 2015) suggesting that cones attempt to metabolize more glucose through aerobic glycolysis. This metabolic reprogramming in cones may be similar to the Warburg effect in cancers where tumors adapt to glucose deprivation (Amoroso et al., 2012). Consistent with this, we found that constitutive activation of the mammalian target of rapamycin complex 1 (mTORC1), through ablation of the tuberous sclerosis complex protein 1 (TSC1), confers a strong survival advantage to cones in *rd1* mice (Venkatesh et al., 2015). mTORC1 regulates aerobic glycolysis. Its constitutive activation further enhanced the expression of the aforementioned genes and of retinal NAPDH levels, likely improving the efficacy and durability of this natural protective mechanism. Moreover, subretinal injection of exogenous glucose (Wang et al., 2016) or overexpression of the rod-derived cone viability factor, which indirectly increases glucose uptake and aerobic glycolysis in cones (Aït-Ali et al., 2015), have both also been shown to improve cone survival, further attributing a central role to glucose during secondary cone death in RP.

We used the Ai9 reporter mice to score for cone survival. Contrary to the cone marker cone arrestin, Cre-mediated expression of td-Tomato in *rd1* cones does not decrease in degenerating cones (Figure S6). At 2 months, we found decreased cone survival in *rd1_Hk2*$^{c/c}$*_MCre*$^{+}$ retinas when compared to *rd1_Hk2*$^{c/+}$*_MCre*$^{+}$ and control retinas (Figure 7). Similarly, HK2 loss abrogated the pro-survival effect of constitutively activated mTORC1 in *rd1_Tsc1*$^{c/c}$*_Hk2*$^{c/c}$*_MCre*$^{+}$ mice (Figures 7B and S7A). In the latter case, the survival effect depended on the dose of *Hk2*. These results demonstrate that improved glucose metabolism mediates cone survival upon TSC1 loss and show that HK2-mediated aerobic glycolysis allows better PR adaptability under the metabolic stress created by the loss of rods in retinitis pigmentosa. Notably, deleting HIF-1a, a key regulator of *Hk2* expression (Riddle et al., 2000) that is upregulated in cones of *rd1* mice and upon TSC1 loss in cones (Punzo et al., 2009; Venkatesh et al., 2015), had no effect on cone survival in *rd1* and *rd1_Tsc1*$^{c/c}$*_MCre*$^{+}$ mice (Figure S7). Thus, HIF-1a does not regulate HK2 in *rd1* and *rd1_Tsc1*$^{c/c}$*_MCre*$^{+}$ cones.

DISCUSSION

Since its initial observations by Otto Warburg, aerobic glycolysis has been documented in nearly all embryonic and rapidly proliferating cells, where it plays a fundamental role in supporting cell growth (Vander Heiden et al., 2009). However, why post-mitotic PRs also perform aerobic glycolysis has remained unclear. In this work, we (1) identified HK2 as a key regulator of aerobic glycolysis in PRs, and (2) revealed the importance of HK2-mediated aerobic glycolysis for PR function and survival *in vivo*. We found that HK2-mediated aerobic glycolysis is not a necessity for PR survival. Yet, aerobic glycolysis is required for optimal rod function and for the survival of nutrient-deprived cones. Based on our data, we propose that aerobic glycolysis is a metabolic choice carried out to maximize overall PR health.

PRs Can Adapt Their Metabolism

We obtained compelling evidence that PRs are able to reprogram their energy metabolism from aerobic glycolysis to increased OXPHOS upon HK2 loss. First, we found that reduction of aerobic glycolysis in HK2-deficient rods does not affect glucose uptake (Figure S5). This suggests that HK2 loss inhibits glycolysis without causing PRs to catabolize alternative energy substrates. Glucose may now be preferentially diverted toward the mitochondria. Second, we found that rods progressively increase the number of their mitochondria when HK2-mediated aerobic glycolysis is inhibited (Figures 5, S2, S3, and S4), probably to generate more ATP. Reduction of aerobic glycolysis in PRs decreases by ~20% the retinal ATP production (Ames et al., 1992; Chinchore et al., 2017; Winkler, 1981), accounting for ~50% of ATP produced by PRs (Chertov et al., 2011). Yet, PR mitochondria operate at full capacity, with limited reserve to generate more ATP. Mitochondria may thus replicate to meet the energy demands of PRs in the absence of HK2. In human neural progenitor cells (Zheng et al., 2016) and hepatocellular carcinoma (DeWaal et al., 2018), HK2 loss also marks the transition from aerobic glycolysis to OXPHOS. In isolated mouse retinas, inhibition of aerobic glycolysis did not change ATP levels, but resulted in a greater fraction of the ATP pool that is sensitive to inhibition of mitochondrial function (Chinchore et al., 2017). While our study documents PR flexibility between aerobic glycolysis and OXPHOS *in vivo*, the mechanisms linking Hk2 loss with decreased LDHA and PKM2 expression (Woo et al., 2015) and enhanced OXPHOS (DeWaal et al., 2018) require still further exploration.

Figure 3. Rod and Cone Survival upon HK2 Loss

(A–D) Analysis of rod survival upon loss of HK2 in rods by fundus photography (A), quantification of total ONL nuclei per section (B), measurements of ONL thickness (C) and IHC on retinal sections (D) (RHO, rhodopsin red signal; PNA, green signal; blue, DAPI).

(E–G) Cone survival analysis upon HK2 loss in cones performed on retinal flat mounts (E and F) stained for cone arrestin (CA) over time and PNA, medium wavelength (L/M) opsin and short wavelength (S) opsin at 1 month (F, cones per retina), and by IHC (G) for cone markers indicated in panels.

Age and genotypes as indicated: blue, DAPI (D and G), removed from 60% of panels to visualize red and green signals. Errors bars ± SD; numbers in bars, number of retinas analyzed; ONL, outer nuclear layer; INL, inner nuclear layer. Scale bars, 85 μm.

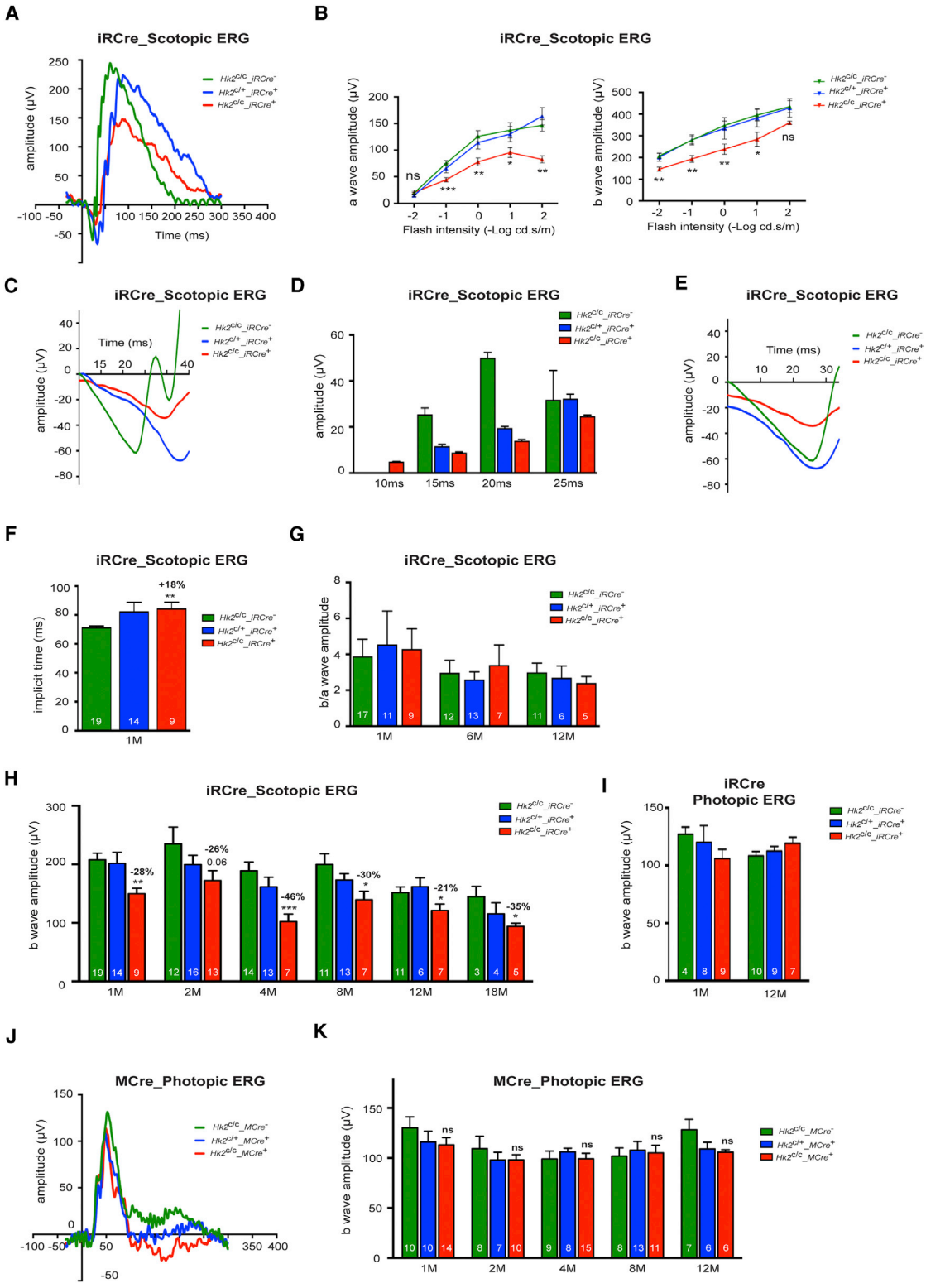

Figure 4. Analysis of Rod and Cone Function upon Loss of HK2

(A–I) Scotopic and photopic ERG recordings upon HK2 loss in rods.

(A) Representative scotopic single-flash (10 cd*s/m^2) ERG responses from 1-month-old mice.

(B) Scotopic ERG a- and b-wave responses from 1-month-old mice recorded over 5 light intensities (*Hk2$^{c/c}$_iRCre$^-$*: n = 17; *Hk2$^{c/+}$_iRCre$^+$*: n = 11; *Hk2$^{c/c}$_iRCre$^-$*: n = 9).

(legend continued on next page)

Interestingly, rods show signs of similar metabolic flexibility with age. At 12 months, we found that HK2 expression was reduced while HK1 expression and mitochondria number increased (Figure S4). In line with our results, lactate production in the mouse retina decreases from 6 to 32 months (Kanow et al., 2017), whereas PR mitochondrial dynamics increases (Kam and Jeffery, 2015). Age-related thickening of the Bruch's membrane may be associated with reduced metabolic exchange that restricts the nutrient supply to PRs (Dithmar et al., 2000). Alternatively, the aging RPE may become more glycolytic, thereby reducing glucose available to PRs (Kanow et al., 2017).

Cones are less dependent on glycolysis than rods as they did not further increase their mitochondrial content upon HK2 loss (Figure S5). This is probably because cones already have a higher capacity for OXPHOS (Perkins et al., 2003), they buffer ATP more efficiently than rods (Rueda et al., 2016), and/or because they can efficiently metabolize other fuels. Accordingly, extreme changes in glucose levels (Macaluso et al., 1992) or iodoacetic acid-mediated inhibition of glycolysis affects rods more than cones (Wang et al., 2011).

Aerobic Glycolysis Is Required for Optimal Rod Function

Interestingly, the increase in the number of mitochondria after HK2 loss in rods did not substitute completely for aerobic glycolysis as seen by the reduction in rod function (Figure 4). This result is in agreement with previous *ex vivo* studies (Winkler, 1981). Aerobic glycolysis in the retina is thought to promote the daily renewal of the PR OS because genetic inhibition of LDHA or PKM2 in rods reduced rod OS length (Chinchore et al., 2017). Enhanced aerobic glycolysis in PRs may allow glucose in excess to be diverged into the pentose phosphate pathway (PPP) for the generation of more NADPH, which is necessary for lipid synthesis and recycling of the visual chromophore. Here, HK2 loss decreased NADPH. Yet, we did not observe appreciable changes in the rod OS length over 12 months (Figures 3 and S3). Another study reported no changes in the OS length upon the conditional depletion of *Pkm2* in rods (Wubben et al., 2017). Upon HK2 loss, HK1 and OXPHOS upregulation may compensate for the reduction of glucose driven biosynthesis through the PPP, by increasing NADPH and tricarboxylic acid (TCA) cycle intermediates used as precursors for fatty acids synthesis (Adler et al., 2014). Upon LDHA loss, this compensatory mechanism may be less present and/or anabolic pathways may be more affected. Consistent with this, we observed that partial or total loss of HK2 in rods did not have the same effects on glucose uptake, glycolytic gene expression and mitochondrial biogenesis, despite a similar reduction in lactate production (Figure 2).

Our data support the hypothesis that aerobic glycolysis is a source of ATP for rod terminal processes (Rueda et al., 2016). Rod synaptic terminal express high levels of HK2, but not HK1, contain high levels of the liver isoform of phosphofructokinase (PFK-L) and high LDH activity, but low cytochrome *c* oxidase activity compared to the IS (Rueda et al., 2016). HK2-depleted rods experience changes in their dark current and/or glutamate vesicle recycling, two ATP-consuming processes (Figure 4). Moreover, HK2-depleted rods exhibit perinuclear mitochondria, which are only seen in avascular retinas where there is a problem for ATP-dependent reactions at the synaptic terminal (Linton et al., 2010; Stone et al., 2008).

Aerobic Glycolysis Contributes to Retinitis Pigmentosa Pathogenesis

Although genetic and environmental factors contribute to PR degenerative diseases, the underlying etiology common to many such diseases may be dysregulated metabolism of these metabolically demanding cells (Aït-Ali et al., 2015; Joyal et al., 2016; Punzo et al., 2009; Venkatesh et al., 2015; Zhang et al., 2016; Zieger and Punzo, 2016). Thus, understanding what PRs need to survive could lead to mutation-independent therapies that could be broadly applicable (Petit et al., 2016). We have provided evidence that HK2-mediated aerobic glycolysis helps cones to adapt to the metabolic stress created by the loss of rod in RP. Our data corroborate previous findings that glucose might be the limiting factor for cone survival during disease. Intuitively it would make more sense that cones make most of the limited glucose through OXPHOS. However, cones prefer to use the glucose available through aerobic glycolysis, maybe because besides ATP, it may also provide most of the NADPH and building blocks required for anabolism. Accordingly, the reduction in cone function in HK2 double mutant mice, suggests that cones may partially rely on other fuels to meet their high ATP needs when under stress (Figure S5). In this regard, we did not observe increased AMP-kinase phosphorylation in *rd1* cones at the onset of cone death (data not shown). The low glucose availability in *rd1* cones likely creates an NAPDH shortage that becomes detrimental. Indeed, we showed that loss of the NADPH-dependent apoptotic *Caspase-2* prolongs cones survival in *rd1* mice, while constitutive mTORC1 activation improved durability of this aerobic glycolysis-driven defense (Venkatesh

(C) Representative scotopic single-flash (10 cd*s/m^2) ERG responses from 1-month-old mice shown at different scales to highlight the a-wave response.
(D) Amplitude of the scotopic a-wave response at fixed time point after flash onset.
(E) Comparison of the leading edge of the scotopic a-wave (10 cd*s/m^2) after normalization (shown are representative responses as in A and C).
(F) Implicit time of b-wave responses at 1 months of age.
(G) b/a-wave amplitude ratios of scotopic ERG recorded at 0.1 cd*s/m^2 at time indicated.
(H) b-wave amplitude of scotopic single-flash ERG responses over time at 0.01 cd*s/m^2.
(I) b-wave amplitude of photopic responses at 1 and 12 months.
(J and K) Photopic ERG recordings upon loss of HK2 in cones.
(J) Representative photopic single-flash responses from 2-month-old mice.
(K) b-wave amplitude of photopic responses over time.
Errors bars ± SD; numbers in bars, number of mice analyzed.

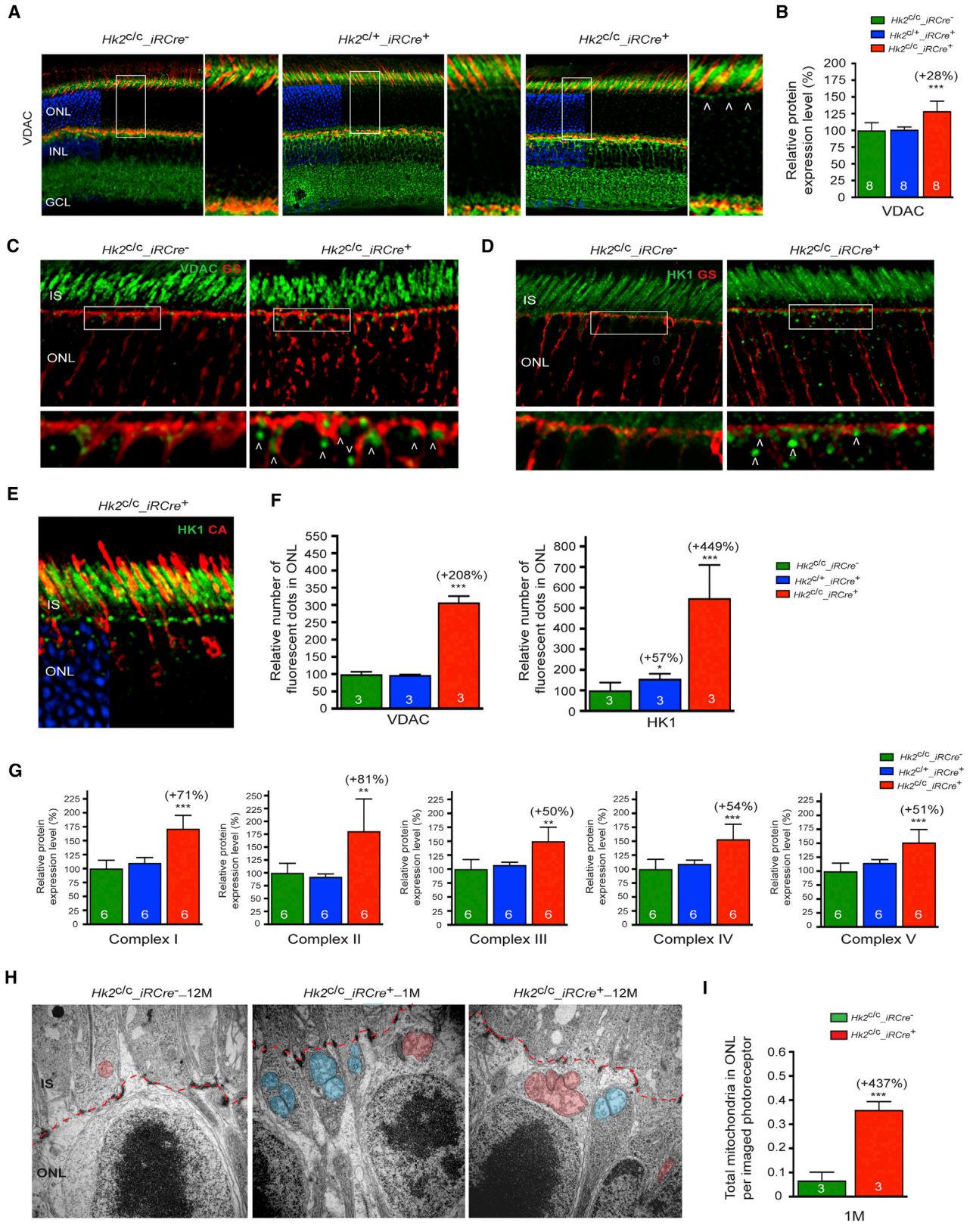

(legend on next page)

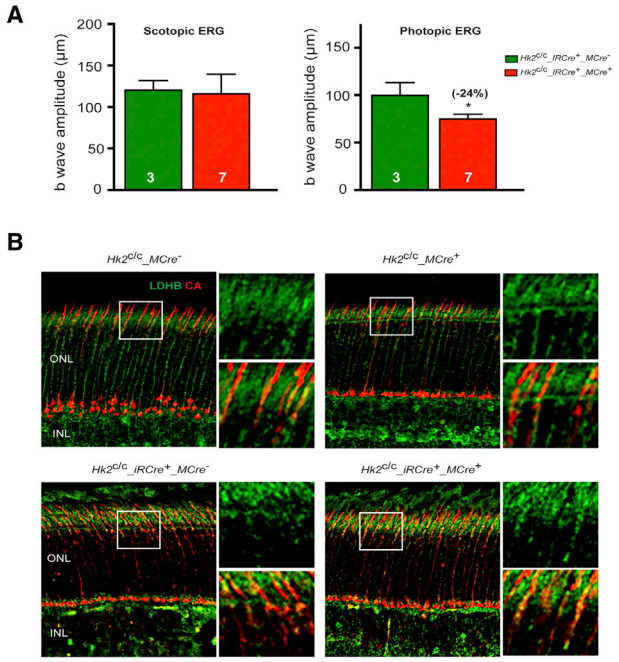

Figure 6. Retinal Function in HK2 Double Knockout Mice

(A) ERG recordings in HK2 double knockout mice at 4 months of age showing no difference in the b-wave amplitudes of scotopic single-flash ERG responses at 0.01 cd*s/m^2 between *Hk2$^{c/c}$_iRCre$^+$* and *Hk2$^{c/c}$_iRCre$^+$_MCre$^+$* littermates. In contrast b-wave amplitudes of photopic responses show reduced cone function only in *iRCre$^+$_MCre$^+$* retinas. Errors bars ± SD; numbers in bars, number of mice analyzed.

(B) Representative IHC images on retinal sections for LDHB expression (green signal) at 1 (top) or 2 (bottom) months of age. Cones were detected with an anti-cone arrestin antibody (CA, red signal). Higher magnification of boxed areas is shown to the right of each panel. INL, inner nuclear layer; ONL, outer nuclear layer.

et al., 2015). Further studies are needed to determine how enhanced aerobic glycolysis enhances NADPH production or consumption. In the meantime, the observation that "forced" aerobic glycolysis in neurons causes detrimental pyruvate depletion and ATP shortage upon limited glucose uptake warrants further examination (Zheng et al., 2016). "Forced" aerobic glycolysis may be both friend and foe to PR survival, depending on the circumstance.

EXPERIMENTAL PROCEDURES

Animals

Ai9 Cre reporter, *Pde6β$^{rd1/rd1}$* (referred as *rd1*), C57BL/6J, *Hif1a$^{c/c}$*, and *Tsc1$^{c/c}$* mice were purchased from Jackson Laboratories. The *Nrl$^{-/-}$* (Mears et al., 2001), the cone-*Cre* mice (referred as M*Cre*) (Le et al., 2004), the rod iCre-75 mice (referred as iR*Cre*) (Li et al., 2005), and the *Hk2$^{c/c}$* mice (Patra et al., 2013) were kindly provided by Drs. H. Khanna, Y.Z. Le, C.K. Chen, and N. Hay, respectively. All animal procedures were approved by the university's Institutional Animal Care and Use Committee (IACUC). Ages of animals varied between 1–12 months as indicated in figures. Male and female mice were used in equal numbers unless indicated.

Electroretinography and Funduscopy

Electroretinography (ERG) and funduscopy were carried out as previously described (Hood and Birch, 1996-1997; Ma et al., 2015; Venkatesh et al., 2013).

Quantification of Cre$^+$ Cells Using Flow Cytometry

Retinas from 2 *Ai9$^{+/+}$_MCre$^+$* mice and 2 *Ai9$^{+/+}$*_iR*Cre$^+$* mice were pooled and dissociated into single cells by papain digestion. Td-Tomato$^+$ cells were quantified using flow cytometry.

Immunohistochemistry

Immunohistochemistry (IHC) was performed on retinal cryosections (20 μm) as described previously (Venkatesh et al., 2013) with a minimum of 3 mice per line. An antibody list is presented in the Supplemental Information.

Quantification of PR Survival

Quantification of rod survival was performed on retinal cross-sections by measuring the thickness of the ONL and counting all ONL nuclei within 3–5 consecutive sections per eye (Petit et al., 2017). Quantification of cone survival was performed on retinal flat-mounts by counting all cones over the entire retinal surface. Antibody staining and tiling of retina was performed as described (Venkatesh et al., 2015). Ai9$^+$, PNA$^+$, LM opsin$^+$, or S opsin$^+$ cones and ONL nuclei were automatically counted using Imaris software.

Transmission Electron Microscopy

Electron microscopy was carried out as previously described (Ma et al., 2015) with 3 mice per line. OS length was measured at multiple locations on semi-thin sections. Mitochondria number per ONL cell was determined on randomly acquired TEM images by counting >200 PR cells per mouse.

Quantitative Western Blots

HK2 expression analysis during development used 4-pooled retinas from 3 mice per time point. The metabolic gene expression analysis used 2-pooled retinas from 1 mouse as one biological sample. Five to 8 biological samples were analyzed per line. Protein extracts from liver of adult C57/Bl6 mice and HEK293 cells were used as negative and positive controls, respectively.

Figure 5. Increased Mitochondria Number upon Loss of HK2 in Rods

(A) Retinal sections showing increased VDAC (green, arrowheads show large VDAC$^+$ dots) expression upon loss of HK2 in rods (red, PNA; blue, DAPI, removed from 60% of panels to visualize red and green signals). Boxed areas are shown to the right of each panel.

(B) Relative levels of VDAC protein assessed by western blot of total retinal extracts.

(C and D) Retinal sections stained for glutamine synthetase (GS, red) and VDAC (C, green) or HK1 (D, green) showing no colocalization of large green dots (arrowhead) with GS. Boxed areas are shown below each panel.

(E) Cross-sections of *Hk2$^{c/c}$_iRCre$^+$* retina showing that HK1 dots (green) do not co-localize with cone arrestin (CA, red; DAPI, blue, removed from 60% of panels to visualize red and green signals).

(F) Relative number of VDAC- or HK1-positive dots in the ONL.

(G) Relative level of the 5 OXPHOS complexes assessed by western blot of total retinal extracts.

(H and I) Transmission electron microscopy images (H) and mitochondria quantification (I) showing a larger number of PR mitochondria (red) in the rod perinuclear region upon loss of HK2 at 1 and 12 months (blue, mitochondria located in Mueller glia processes; red dotted line, outer limiting membrane).

Age in all experiments: 1 month except as indicated in (H); genotypes as indicated; results in (B), (F), and (G): % of wild-type. Error bars ± SD; numbers in bars, number of biological samples; ONL, outer nuclear layer; INL, inner nuclear layer; IS, inner segment; GCL, ganglion cell layer.

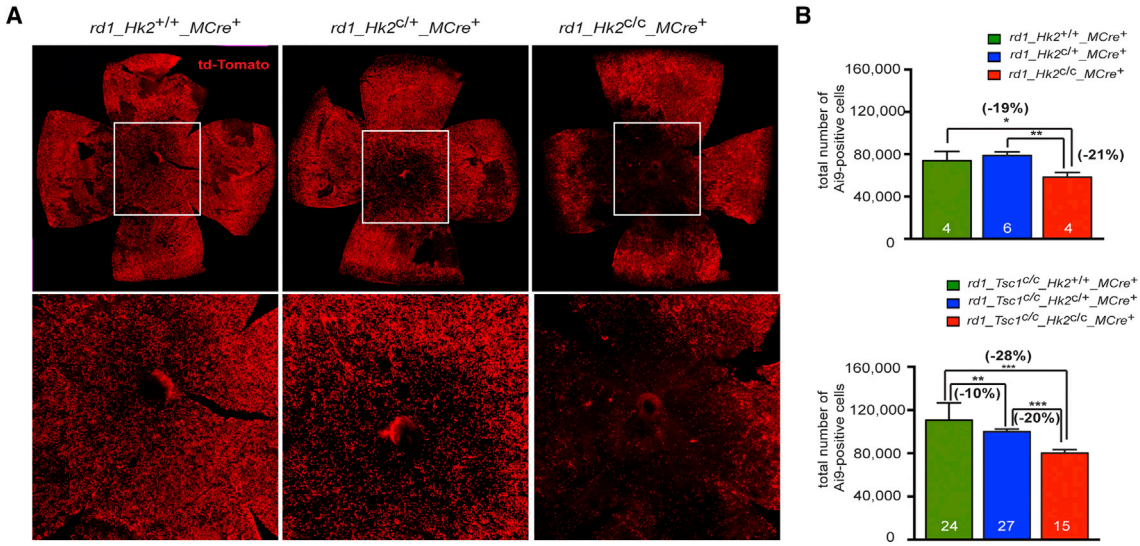

Figure 7. HK2 Promotes Cone Survival in Retinitis Pigmentosa

(A) Representative retinal flat mounts at 2 months of genotypes indicated showing less central *Ai9*$^+$ cones upon loss of HK2 in cones (higher magnification of boxed area).

(B) Quantification of the total number of *Ai9*$^+$ cones per retina at 2 months in genotypes indicated. Errors bars ± SD; numbers in bars, number of retinas analyzed.

Protein extracts were prepared as described (Petit et al., 2012). Detailed procedures and antibodies are presented in the Supplemental Information.

Real-Time qPCR

Retinas from one mouse were pooled to isolate total RNA using TRIzol (Invitro Life Technologies). Total RNA was treated with DNase I, reverse-transcribed using random hexamer primers, and real-time qPCR was performed using a Bio-Rad CFX96. Two to 3 biological samples were analyzed per line. Primers and protocols are presented in the Supplemental Information.

Glucose Uptake Assay

Retinas were dissected in cold DMEM, cultured for 45 min at 37°C in DMEM medium with or without D-glucose in the presence of the fluorescent glucose analog 2-deoxy-D-glucose (2-NBDG, 1 μM), washed 4 times with ice-cold PBS and DAPI, flat-mounted between 2 pre-chilled cover slides, and imaged immediately (<10 min). Images were taken at the level of the PR segments at 5 different locations. Measurements represent duplicates of 2 experiments each.

Lactate and NADPH Assay

Lactate (Lactate assay kit: Eton Bioscience) and NADPH (Fluoro NADP/NADPH: Cell Technology) assays were performed in triplicate using 2–3 biological samples, with each biological sample consisting of 2 retinas. Retinas were dissected in ice cold DMEM, rinsed in PBS, sonicated in assay buffer, and processed following manufacturer's instructions. Results were normalized per retina.

Statistical Analysis

The Student's t test was used with following significance levels: *$p < 0.05$; **$p < 0.01$; ***$p < 0.0001$. Bar graphs indicate mean and SD. Required sample sizes were determined using G*Power 3.1 based on the effect sizes obtained with two *Cre*$^+$ and two *Cre*$^-$ biological samples (each containing 2 retinas from 1 animal). Test conditions: $\alpha = 0.05$, power = 0.9. Biological samples used for sample size calculation were added to the final n numbers. Achieved power was >0.92 for all tests, except for expression changes of GLUT1 (0.535) and Complex II (0.879).

SUPPLEMENTAL INFORMATION

Supplemental Information includes Supplemental Experimental Procedures and seven figures and can be found with this article online at https://doi.org/10.1016/j.celrep.2018.04.111.

ACKNOWLEDGMENTS

We are grateful to Hemant Khanna, Yun Z. Le, and Ching-Kang Chen for providing reagents. This work was supported by a grant from the "Information Recherche Retinite Pigmentaire" Association (to L.P.) and by the US NIH (R01-EY023570 to C.P. and R01-CA206167 to N.H.). L.P. acknowledges the Fulbright/Fondation Monahan Postdoctoral Fellowship, the Fondation de France "Young researcher in ophthalmology" Fellowship, and the Association Française contre les Myopathies Postdoctoral Fellowship. N.H. acknowledges the VA Merit Award BX000733.

AUTHOR CONTRIBUTIONS

L.P. conceived and performed experiments, interpreted data, and wrote the manuscript. J.C., S.-Y.C., and S.M. performed experiments. M.Z. provided feedback. N.H. provided reagents. C.P. conceived and performed experiments and wrote the manuscript.

DECLARATION OF INTERESTS

The authors declare no competing interests.

Received: August 15, 2017
Revised: March 22, 2018
Accepted: April 25, 2018
Published: May 29, 2018

REFERENCES

Adler, L., 4th, Chen, C., and Koutalos, Y. (2014). Mitochondria contribute to NADPH generation in mouse rod photoreceptors. J. Biol. Chem. *289*, 1519–1528.

Aït-Ali, N., Fridlich, R., Millet-Puel, G., Clérin, E., Delalande, F., Jaillard, C., Blond, F., Perrocheau, L., Reichman, S., Byrne, L.C., et al. (2015). Rod-derived cone viability factor promotes cone survival by stimulating aerobic glycolysis. Cell *161*, 817–832.

Ames, A., 3rd. (2000). CNS energy metabolism as related to function. Brain Res. Brain Res. Rev. *34*, 42–68.

Ames, A., 3rd, Li, Y.Y., Heher, E.C., and Kimble, C.R. (1992). Energy metabolism of rabbit retina as related to function: high cost of Na+ transport. J. Neurosci. *12*, 840–853.

Amoroso, F., Falzoni, S., Adinolfi, E., Ferrari, D., and Di Virgilio, F. (2012). The P2X7 receptor is a key modulator of aerobic glycolysis. Cell Death Dis. *3*, e370.

Arora, K.K., and Pedersen, P.L. (1988). Functional significance of mitochondrial bound hexokinase in tumor cell metabolism. Evidence for preferential phosphorylation of glucose by intramitochondrially generated ATP. J. Biol. Chem. *263*, 17422–17428.

Casson, R.J., Wood, J.P., Han, G., Kittipassorn, T., Peet, D.J., and Chidlow, G. (2016). M-type pyruvate kinase isoforms and lactate dehydrogenase A in the mammalian retina: metabolic implications. Invest. Ophthalmol. Vis. Sci. *57*, 66–80.

Chertov, A.O., Holzhausen, L., Kuok, I.T., Couron, D., Parker, E., Linton, J.D., Sadilek, M., Sweet, I.R., and Hurley, J.B. (2011). Roles of glucose in photoreceptor survival. J. Biol. Chem. *286*, 34700–34711.

Chinchore, Y., Begaj, T., Wu, D., Drokhlyansky, E., and Cepko, C.L. (2017). Glycolytic reliance promotes anabolism in photoreceptors. eLife *6*, e25946.

Cohen, L.H., and Noell, W.K. (1960). Glucose catabolism of rabbit retina before and after development of visual function. J. Neurochem. *5*, 253–276.

DeWaal, D., Nogueira, V., Terry, A.R., Patra, K.C., Jeon, S.M., Guzman, G., Au, J., Long, C.P., Antoniewicz, M.R., and Hay, N. (2018). Hexokinase-2 depletion inhibits glycolysis and induces oxidative phosphorylation in hepatocellular carcinoma and sensitizes to metformin. Nat. Commun. *9*, 446.

Dithmar, S., Curcio, C.A., Le, N.A., Brown, S., and Grossniklaus, H.E. (2000). Ultrastructural changes in Bruch's membrane of apolipoprotein E-deficient mice. Invest. Ophthalmol. Vis. Sci. *41*, 2035–2042.

Gershon, T.R., Crowther, A.J., Tikunov, A., Garcia, I., Annis, R., Yuan, H., Miller, C.R., Macdonald, J., Olson, J., and Deshmukh, M. (2013). Hexokinase-2-mediated aerobic glycolysis is integral to cerebellar neurogenesis and pathogenesis of medulloblastoma. Cancer Metab. *1*, 2.

Hoang, Q.V., Linsenmeier, R.A., Chung, C.K., and Curcio, C.A. (2002). Photoreceptor inner segments in monkey and human retina: mitochondrial density, optics, and regional variation. Vis. Neurosci. *19*, 395–407.

Hood, D.C., and Birch, D.G. (1996-1997). Assessing abnormal rod photoreceptor activity with the a-wave of the electroretinogram: applications and methods. Doc. Ophthalmol. *92*, 253–267.

Hurley, J.B., Lindsay, K.J., and Du, J. (2015). Glucose, lactate, and shuttling of metabolites in vertebrate retinas. J. Neurosci. Res. *93*, 1079–1092.

Iqbal, M.A., Siddiqui, F.A., Gupta, V., Chattopadhyay, S., Gopinath, P., Kumar, B., Manvati, S., Chaman, N., and Bamezai, R.N. (2013). Insulin enhances metabolic capacities of cancer cells by dual regulation of glycolytic enzyme pyruvate kinase M2. Mol. Cancer *12*, 72.

Iqbal, M.A., Gupta, V., Gopinath, P., Mazurek, S., and Bamezai, R.N. (2014). Pyruvate kinase M2 and cancer: an updated assessment. FEBS Lett. *588*, 2685–2692.

Joyal, J.S., Sun, Y., Gantner, M.L., Shao, Z., Evans, L.P., Saba, N., Fredrick, T., Burnim, S., Kim, J.S., Patel, G., et al. (2016). Retinal lipid and glucose metabolism dictates angiogenesis through the lipid sensor Ffar1. Nat. Med. *22*, 439–445.

Kam, J.H., and Jeffery, G. (2015). To unite or divide: mitochondrial dynamics in the murine outer retina that preceded age related photoreceptor loss. Oncotarget *6*, 26690–26701.

Kanow, M.A., Giarmarco, M.M., Jankowski, C.S., Tsantilas, K., Engel, A.L., Du, J., Linton, J.D., Farnsworth, C.C., Sloat, S.R., Rountree, A., et al. (2017). Biochemical adaptations of the retina and retinal pigment epithelium support a metabolic ecosystem in the vertebrate eye. eLife *6*, e28899.

LaVail, M.M. (1976). Rod outer segment disk shedding in rat retina: relationship to cyclic lighting. Science *194*, 1071–1074.

Le, Y.Z., Ash, J.D., Al-Ubaidi, M.R., Chen, Y., Ma, J.X., and Anderson, R.E. (2004). Targeted expression of Cre recombinase to cone photoreceptors in transgenic mice. Mol. Vis. *10*, 1011–1018.

Li, S., Chen, D., Sauvé, Y., McCandless, J., Chen, Y.J., and Chen, C.K. (2005). Rhodopsin-iCre transgenic mouse line for Cre-mediated rod-specific gene targeting. Genesis *41*, 73–80.

Linton, J.D., Holzhausen, L.C., Babai, N., Song, H., Miyagishima, K.J., Stearns, G.W., Lindsay, K., Wei, J., Chertov, A.O., Peters, T.A., et al. (2010). Flow of energy in the outer retina in darkness and in light. Proc. Natl. Acad. Sci. USA *107*, 8599–8604.

Ma, S., Venkatesh, A., Langellotto, F., Le, Y.Z., Hall, M.N., Rüegg, M.A., and Punzo, C. (2015). Loss of mTOR signaling affects cone function, cone structure and expression of cone specific proteins without affecting cone survival. Exp. Eye Res. *135*, 1–13.

Macaluso, C., Onoe, S., and Niemeyer, G. (1992). Changes in glucose level affect rod function more than cone function in the isolated, perfused cat eye. Invest. Ophthalmol. Vis. Sci. *33*, 2798–2808.

Mathupala, S.P., Rempel, A., and Pedersen, P.L. (1997). Aberrant glycolytic metabolism of cancer cells: a remarkable coordination of genetic, transcriptional, post-translational, and mutational events that lead to a critical role for type II hexokinase. J. Bioenerg. Biomembr. *29*, 339–343.

Mathupala, S.P., Ko, Y.H., and Pedersen, P.L. (2006). Hexokinase II: cancer's double-edged sword acting as both facilitator and gatekeeper of malignancy when bound to mitochondria. Oncogene *25*, 4777–4786.

Mears, A.J., Kondo, M., Swain, P.K., Takada, Y., Bush, R.A., Saunders, T.L., Sieving, P.A., and Swaroop, A. (2001). Nrl is required for rod photoreceptor development. Nat. Genet. *29*, 447–452.

Mergenthaler, P., Kahl, A., Kamitz, A., van Laak, V., Stohlmann, K., Thomsen, S., Klawitter, H., Przesdzing, I., Neeb, L., Freyer, D., et al. (2012). Mitochondrial hexokinase II (HKII) and phosphoprotein enriched in astrocytes (PEA15) form a molecular switch governing cellular fate depending on the metabolic state. Proc. Natl. Acad. Sci. USA *109*, 1518–1523.

Mergenthaler, P., Lindauer, U., Dienel, G.A., and Meisel, A. (2013). Sugar for the brain: the role of glucose in physiological and pathological brain function. Trends Neurosci. *36*, 587–597.

Narayan, D.S., Chidlow, G., Wood, J.P., and Casson, R.J. (2017). Glucose metabolism in mammalian photoreceptor inner and outer segments. Clin. Experiment. Ophthalmol. *45*, 730–741.

Nikonov, S.S., Brown, B.M., Davis, J.A., Zuniga, F.I., Bragin, A., Pugh, E.N., Jr., and Craft, C.M. (2008). Mouse cones require an arrestin for normal inactivation of phototransduction. Neuron *59*, 462–474.

Okawa, H., Sampath, A.P., Laughlin, S.B., and Fain, G.L. (2008). ATP consumption by mammalian rod photoreceptors in darkness and in light. Curr. Biol. *18*, 1917–1921.

Patra, K.C., Wang, Q., Bhaskar, P.T., Miller, L., Wang, Z., Wheaton, W., Chandel, N., Laakso, M., Muller, W.J., Allen, E.L., et al. (2013). Hexokinase 2 is required for tumor initiation and maintenance and its systemic deletion is therapeutic in mouse models of cancer. Cancer Cell *24*, 213–228.

Pellerin, L., and Magistretti, P.J. (1994). Glutamate uptake into astrocytes stimulates aerobic glycolysis: a mechanism coupling neuronal activity to glucose utilization. Proc. Natl. Acad. Sci. USA *91*, 10625–10629.

Perkins, G.A., Ellisman, M.H., and Fox, D.A. (2003). Three-dimensional analysis of mouse rod and cone mitochondrial cristae architecture: bioenergetic and functional implications. Mol. Vis. *9*, 60–73.

Petit, L., Lhériteau, E., Weber, M., Le Meur, G., Deschamps, J.Y., Provost, N., Mendes-Madeira, A., Libeau, L., Guihal, C., Colle, M.A., et al. (2012). Restoration of vision in the pde6β-deficient dog, a large animal model of rod-cone dystrophy. Mol. Ther. *20*, 2019–2030.

Petit, L., Khanna, H., and Punzo, C. (2016). Advances in gene therapy for diseases of the eye. Hum. Gene Ther. *27*, 563–579.

Petit, L., Ma, S., Cheng, S.Y., Gao, G., and Punzo, C. (2017). Rod outer segment development influences AAV-mediated photoreceptor transduction after subretinal injection. Hum. Gene Ther. *28*, 464–481.

Poitry-Yamate, C.L., Poitry, S., and Tsacopoulos, M. (1995). Lactate released by Müller glial cells is metabolized by photoreceptors from mammalian retina. J. Neurosci. *15*, 5179–5191.

Punzo, C., Kornacker, K., and Cepko, C.L. (2009). Stimulation of the insulin/mTOR pathway delays cone death in a mouse model of retinitis pigmentosa. Nat. Neurosci. *12*, 44–52.

Rajala, A., Gupta, V.K., Anderson, R.E., and Rajala, R.V. (2013). Light activation of the insulin receptor regulates mitochondrial hexokinase. A possible mechanism of retinal neuroprotection. Mitochondrion *13*, 566–576.

Read, J.A., Winter, V.J., Eszes, C.M., Sessions, R.B., and Brady, R.L. (2001). Structural basis for altered activity of M- and H-isozyme forms of human lactate dehydrogenase. Proteins *43*, 175–185.

Reidel, B., Thompson, J.W., Farsiu, S., Moseley, M.A., Skiba, N.P., and Arshavsky, V.Y. (2011). Proteomic profiling of a layered tissue reveals unique glycolytic specializations of photoreceptor cells. Mol. Cell Proteomics *10*, M110.002469.

Rempel, A., Mathupala, S.P., Griffin, C.A., Hawkins, A.L., and Pedersen, P.L. (1996). Glucose catabolism in cancer cells: amplification of the gene encoding type II hexokinase. Cancer Res. *56*, 2468–2471.

Riddle, S.R., Ahmad, A., Ahmad, S., Deeb, S.S., Malkki, M., Schneider, B.K., Allen, C.B., and White, C.W. (2000). Hypoxia induces hexokinase II gene expression in human lung cell line A549. Am. J. Physiol. Lung Cell. Mol. Physiol. *278*, L407–L416.

Roberts, D.J., and Miyamoto, S. (2015). Hexokinase II integrates energy metabolism and cellular protection: Akting on mitochondria and TORCing to autophagy. Cell Death Differ. *22*, 248–257.

Roberts, D.J., Tan-Sah, V.P., Smith, J.M., and Miyamoto, S. (2013). Akt phosphorylates HK-II at Thr-473 and increases mitochondrial HK-II association to protect cardiomyocytes. J. Biol. Chem. *288*, 23798–23806.

Rueda, E.M., Johnson, J.E., Jr., Giddabasappa, A., Swaroop, A., Brooks, M.J., Sigel, I., Chaney, S.Y., and Fox, D.A. (2016). The cellular and compartmental profile of mouse retinal glycolysis, tricarboxylic acid cycle, oxidative phosphorylation, and ~P transferring kinases. Mol. Vis. *22*, 847–885.

Stone, J., van Driel, D., Valter, K., Rees, S., and Provis, J. (2008). The locations of mitochondria in mammalian photoreceptors: relation to retinal vasculature. Brain Res. *1189*, 58–69.

Valvona, C.J., Fillmore, H.L., Nunn, P.B., and Pilkington, G.J. (2016). The Regulation and Function of Lactate Dehydrogenase A: Therapeutic Potential in Brain Tumor. Brain Pathol. *26*, 3–17.

Vander Heiden, M.G., Cantley, L.C., and Thompson, C.B. (2009). Understanding the Warburg effect: the metabolic requirements of cell proliferation. Science *324*, 1029–1033.

Venkatesh, A., Ma, S., Langellotto, F., Gao, G., and Punzo, C. (2013). Retinal gene delivery by rAAV and DNA electroporation. Curr. Protoc. Microbiol. *Chapter 14*, Unit 14D.14.

Venkatesh, A., Ma, S., Le, Y.Z., Hall, M.N., Rüegg, M.A., and Punzo, C. (2015). Activated mTORC1 promotes long-term cone survival in retinitis pigmentosa mice. J. Clin. Invest. *125*, 1446–1458.

Wang, L., Kondo, M., and Bill, A. (1997). Glucose metabolism in cat outer retina. Effects of light and hyperoxia. Invest. Ophthalmol. Vis. Sci. *38*, 48–55.

Wang, W., Fernandez de Castro, J., Vukmanic, E., Zhou, L., Emery, D., Demarco, P.J., Kaplan, H.J., and Dean, D.C. (2011). Selective rod degeneration and partial cone inactivation characterize an iodoacetic acid model of Swine retinal degeneration. Invest. Ophthalmol. Vis. Sci. *52*, 7917–7923.

Wang, W., Lee, S.J., Scott, P.A., Lu, X., Emery, D., Liu, Y., Ezashi, T., Roberts, M.R., Ross, J.W., Kaplan, H.J., and Dean, D.C. (2016). Two-step reactivation of dormant cones in retinitis pigmentosa. Cell Rep. *15*, 372–385.

Wilson, J.E. (2003). Isozymes of mammalian hexokinase: structure, subcellular localization and metabolic function. J. Exp. Biol. *206*, 2049–2057.

Winkler, B.S. (1981). Glycolytic and oxidative metabolism in relation to retinal function. J. Gen. Physiol. *77*, 667–692.

Wolf, A., Agnihotri, S., Micallef, J., Mukherjee, J., Sabha, N., Cairns, R., Hawkins, C., and Guha, A. (2011). Hexokinase 2 is a key mediator of aerobic glycolysis and promotes tumor growth in human glioblastoma multiforme. J. Exp. Med. *208*, 313–326.

Woo, Y.M., Shin, Y., Lee, E.J., Lee, S., Jeong, S.H., Kong, H.K., Park, E.Y., Kim, H.K., Han, J., Chang, M., and Park, J.H. (2015). Inhibition of aerobic glycolysis represses Akt/mTOR/HIF-1α axis and restores tamoxifen sensitivity in antiestrogen-resistant breast cancer cells. PLoS ONE *10*, e0132285.

Wubben, T.J., Pawar, M., Smith, A., Toolan, K., Hager, H., and Besirli, C.G. (2017). Photoreceptor metabolic reprogramming provides survival advantage in acute stress while causing chronic degeneration. Sci. Rep. *7*, 17863.

Zhang, L., Du, J., Justus, S., Hsu, C.W., Bonet-Ponce, L., Wu, W.H., Tsai, Y.T., Wu, W.P., Jia, Y., Duong, J.K., et al. (2016). Reprogramming metabolism by targeting sirtuin 6 attenuates retinal degeneration. J. Clin. Invest. *126*, 4659–4673.

Zheng, X., Boyer, L., Jin, M., Mertens, J., Kim, Y., Ma, L., Ma, L., Hamm, M., Gage, F.H., and Hunter, T. (2016). Metabolic reprogramming during neuronal differentiation from aerobic glycolysis to neuronal oxidative phosphorylation. eLife *5*, e13374.

Zieger, M., and Punzo, C. (2016). Improved cell metabolism prolongs photoreceptor survival upon retinal-pigmented epithelium loss in the sodium iodate induced model of geographic atrophy. Oncotarget *7*, 9620–9633.

Cell Reports, Volume *23*

Supplemental Information

Aerobic Glycolysis Is Essential for Normal Rod Function and Controls Secondary Cone Death in Retinitis Pigmentosa

Lolita Petit, Shan Ma, Joris Cipi, Shun-Yun Cheng, Marina Zieger, Nissim Hay, and Claudio Punzo

Supplemental Figures

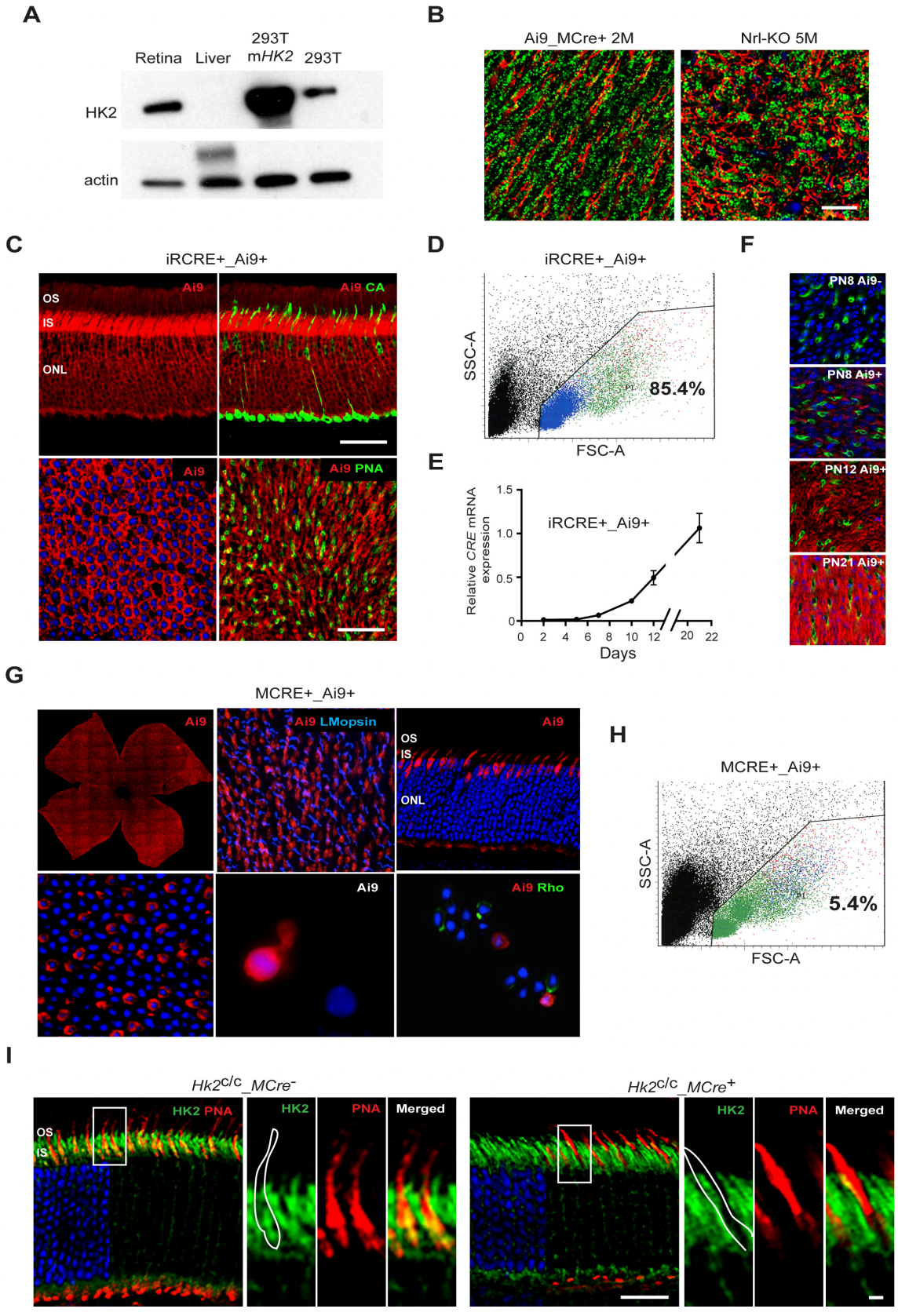

Figure S1. HK2 antibody validation, verification of HK2 expression in cones and analysis of CRE recombinase expression in iR*Cre*$^{+}$ and M*Cre*$^{+}$ mouse retina, Related to Figure 1.

(A) Western-blot analysis detecting HK2 expression in lysates obtained from murine retinas, murine liver, 293T cells transfected with a plasmid expressing the murine *Hk2* cDNA (pAAV-CMV-m*Hk2*) and 293T control cells. No band is detected in the liver extract.

(B) Immunofluorescence analysis of HK2 expression (green signal) on flatmounts of *Ai9_MCre*$^{+}$ and *Nrl*$^{-/-}$ mice at ages indicated. Td-Tomato (first panel red signal) and PNA (second panel red signal) mark cones; DAPI (blue signal) marks nuclei. Scale bar = 25μm.

(C-H) To characterize CRE expression in iR*Cre*$^{+}$ (C-F) and M*Cre*$^{+}$ (G, H) mice, iR*Cre*$^{+}$ and M*Cre*$^{+}$ mice were crossed with the floxed tdTomato reporter line Ai9 (red signal in C, F and G), resulting in iR*Cre*$^{+}$_Ai9^{+} mice and MCre^{+}_Ai9^{+} mice.

(C) Microscopy images of retinal sections and flatmounts stained for cone markers (mouse cone arrestin, CA or PNA, green) or nuclei (DAPI, blue). Almost all cells in the ONL report CRE expression (Ai9^{+}: red), except cones, as previously described (Li et al., 2005). Scale bar: 40μm.

(D) Quantification of td-Tomato positive cells by flow cytometry using standard forward (FSC) and sideward (SSC) settings. Number in graph indicates the percentage of td-Tomato positive cells (blue) in the selected population (green, containing ~90% of rod nuclei, which form a distinct subpopulation with low FSC and SSC (Feodorova et al., 2015)).

(E) Relative CRE expression in retinal extracts at indicated postnatal ages (RT-qPCR). CRE expression is first detected by PN5.

(F) Conditional td-Tomato expression in retinal flatmounts at indicated postnatal ages (fluorescent microscopy). Td-Tomato expression is detected at PN8 and increases overtime (green: PNA; blue: DAPI)..

(G) From top left to bottom right: Tiled retinal flat mount showing uniform distribution of td-Tomato expression across the entire retina. Higher magnification showing td-Tomato expression in cones only (M/L opsin: blue). Retinal cross section showing td-Tomato expression in cones by location in the ONL. Retinal flat mount showing td-Tomato expression in sparse PR nuclei. A Td-Tomato positive cone cell next to another retinal cell after retinal cell dissociation. Td-Tomato positive cones after retinal cell dissociation next to rods stained for rhodopsin (green; blue: DAPI).

(H) Quantification of td-Tomato positive cells by flow cytometry using standard FSC and SSC settings. Number in graph indicates the percentage of td-Tomato positive cells (blue) in the selected population (green: containing ~5% of PR nuclei corresponding to cones).

(I) Immunofluorescence analysis on retinal sections of 1-month-old animals showing complete loss of HK2 (green signal) in inner segments of *MCre*$^{+}$ cones. Higher magnification of boxed areas is shown on the right of each panel (red: PNA; blue: DAPI, removed from 60% of panels to visualize red and green signal). Scale bars: left panel 25μm and right panel 5μm; IS: inner segments; ONL: outer nuclear layer; OS: outer segments.

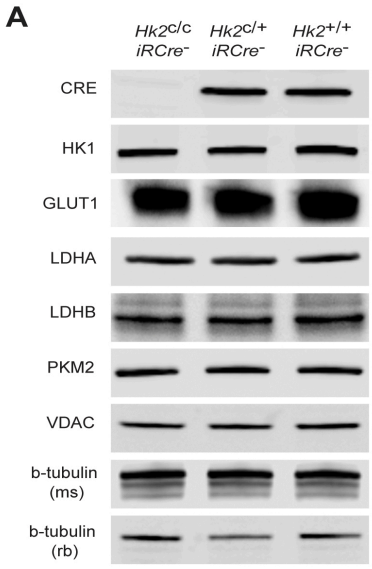

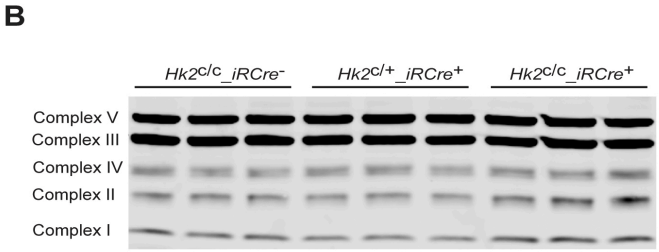

C

	HK2c/c_Cre-		HK2c/+_Cre+		HK2c/c_Cre+		HK2c/c_Cre- versus HK2c/c_Cre+		
	Mean	SD	Mean	SD	Mean	SD	Effect size	Recommended n/group	Actual n
VDAC_old data	100	13.56	95.33	8.69	115.5	7.268	1.36	11	2
VDAC_new data	100	11.65	101.2	13.8	128.7	15.06	2.13	6	8
HK1_old data	100	8.832	125	28.01	145.8	39.63	1.59	10	2
HK1_new data	100	10.64	109.9	26.8	148.1	33.42	1.93	7	7
PKM2_old data	100	2.66	95.54	6.62	75.22	4.25	6.98	2	2
PKM2_new data	100	4.295	96.58	8.535	84.32	8.721	2.28	6	4
LDHA_old data	100	12	30.91	10.44	67.78	10.15	2.89	4	2
LDHA_new data	100	10.55	46.53	27.11	72.87	11.27	2.48	5	5
LDHB_old data	100	17.24	98.67	3.512	97.33	11.59	0.18		
LDHB_new data	100	25.91	101.1	5.93	108.4	23.19	0.34		
GLUT1_old data	100	2.219	84	11.99	127.2	19.79	1.93	7	2
GLUT1_new data	100	8.451	93.76	24.42	123.4	26.24	1.2	16	5
Complex I_new data	100	15.16	110.1	29	171.7	23.73	3.6	3	6
Complex II_new data	100	18.68	92.49	16.57	181	62.67	1.75	8	6
Complex III_new data	100	17.14	107.4	15.46	150	24.99	2.33	5	6
Complex IV_new data	100	17.52	109.6	21.12	153.6	26.82	2.36	5	6
Complex V_new data	100	14.54	114.9	18.07	151.4	23.23	2.65	5	6

Figure S2. Western-blots analyses at 1 month of age, Related to Figures 2 and 5.
(A-B) Examples of western-blots for protein indicated on the left of each row. Genotypes: on the tope of each lane.
(A) Example showing one biological sample per genotype. CRE was included as a genotype control to verify the correct genotype of all samples used. Beta-tubulin (from mouse and/or rabbit) was used as a loading control. Color images obtained using infrared-dye-labeled secondary antibody were exported as black and white images.
(B) Examples showing 3 biological samples per genotype.
(C) Table showing sample size and power analysis. Required sample sizes were determined using G*Power 3.1 based on the effect sizes obtained with two Cre^{+} and two Cre^{-} biological samples (each containing 2 retinas from 1 animal: old data). Conditions of test: α=0.05, power=0.9). The biological samples used for sample size calculation were included in the final (actual) n number of each test. Achieved power was >0.92 for all tests, except for changes in the level of expression of GLUT1 (0.535) and Complex II proteins (0.879).

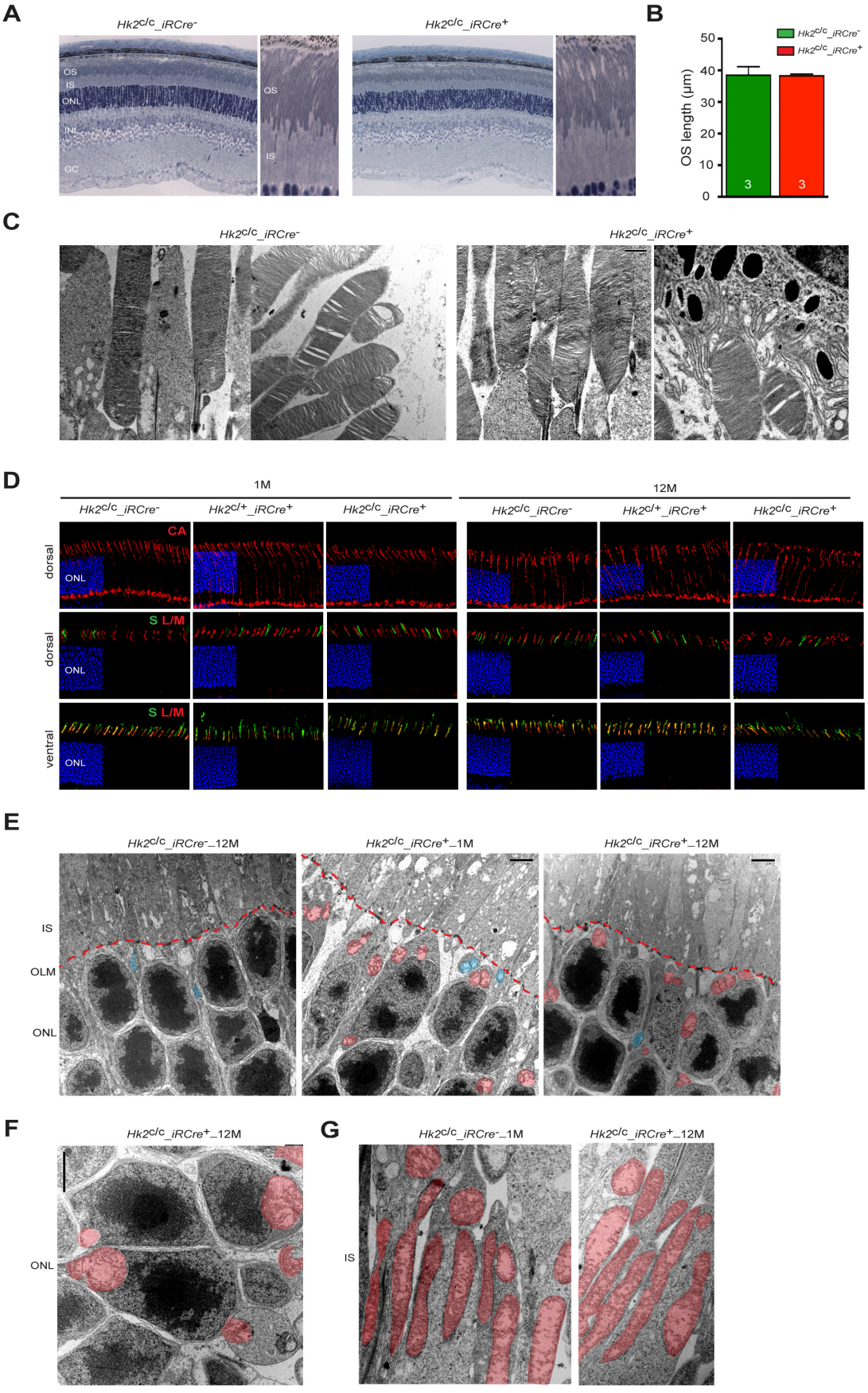
A
Hk2c/c_iRCre-
Hk2c/c_iRCre+
OS
IS
ONL
INL
GC
B
Hk2c/c_iRCre-
Hk2c/c_iRCre+
OS length (μm)
50
40
30
20
10
0
3
3
C
Hk2c/c_iRCre-
Hk2c/c_iRCre+
D
1M
12M
Hk2c/c_iRCre-
Hk2c/+_iRCre+
Hk2c/c_iRCre+
CA
S L/M
dorsal
ventral
ONL
E
Hk2c/c_iRCre-_12M
Hk2c/c_iRCre+_1M
Hk2c/c_iRCre+_12M
IS
OLM
ONL
F
Hk2c/c_iRCre+_12M
ONL
G
Hk2c/c_iRCre-_1M
Hk2c/c_iRCre+_12M
IS

Figure S3. Histological analyses upon loss of HK2 in rods, Related to Figures 3 and 5.
(A) Representative toluidine-stained semi-thin retinal sections showing preservation of rod inner/outer segments upon loss of HK2 in rods.
(B) Quantification of OS length. Errors bars ± SD; Numbers in bars: number of retinas analyzed (each from one different animal).
(C) Electron microscopy images showing rod OS structure of 12-month-old animals. Rod OS are not altered by the loss of HK2 in rods.
(D) Analysis of rod and cone markers upon loss of HK2 in rods performed on dorsal and ventral retinal sections at 1 and 12 months of age using cone arrestin (CA), medium wavelength (L/M) and short wavelength (S) opsin. Because S-opsin is expressed mainly ventrally few S cones are seen on dorsal sections (blue: DAPI, removed from 60% of panels to visualize red and green signals).
(E-G) Representative electron microscopy images of (E) the outer limiting membrane region, (E, F) PR cell nuclei and (G) PR IS from mice of the indicated genotype and age. PR mitochondria are shown in red. Glial mitochondria are shown in blue. The red dotted line represents the outer limiting membrane (identified by the presence of dark adherent junctions). Upon loss of HK2 in rods, cluster of mitochondria are observed in rod perinuclear soma. The number and size of rod perinuclear mitochondria increase with age. There is no apparent change in the size and number of mitochondria in PR inner segments upon loss of HK2, however absolute quantification was not possible due to the very high density of mitochondria in the inner segment. IS: inner segments; INL: inner nuclear layer; OS: outer segments; OLM: outer limiting membrane, ONL: outer nuclear layer.

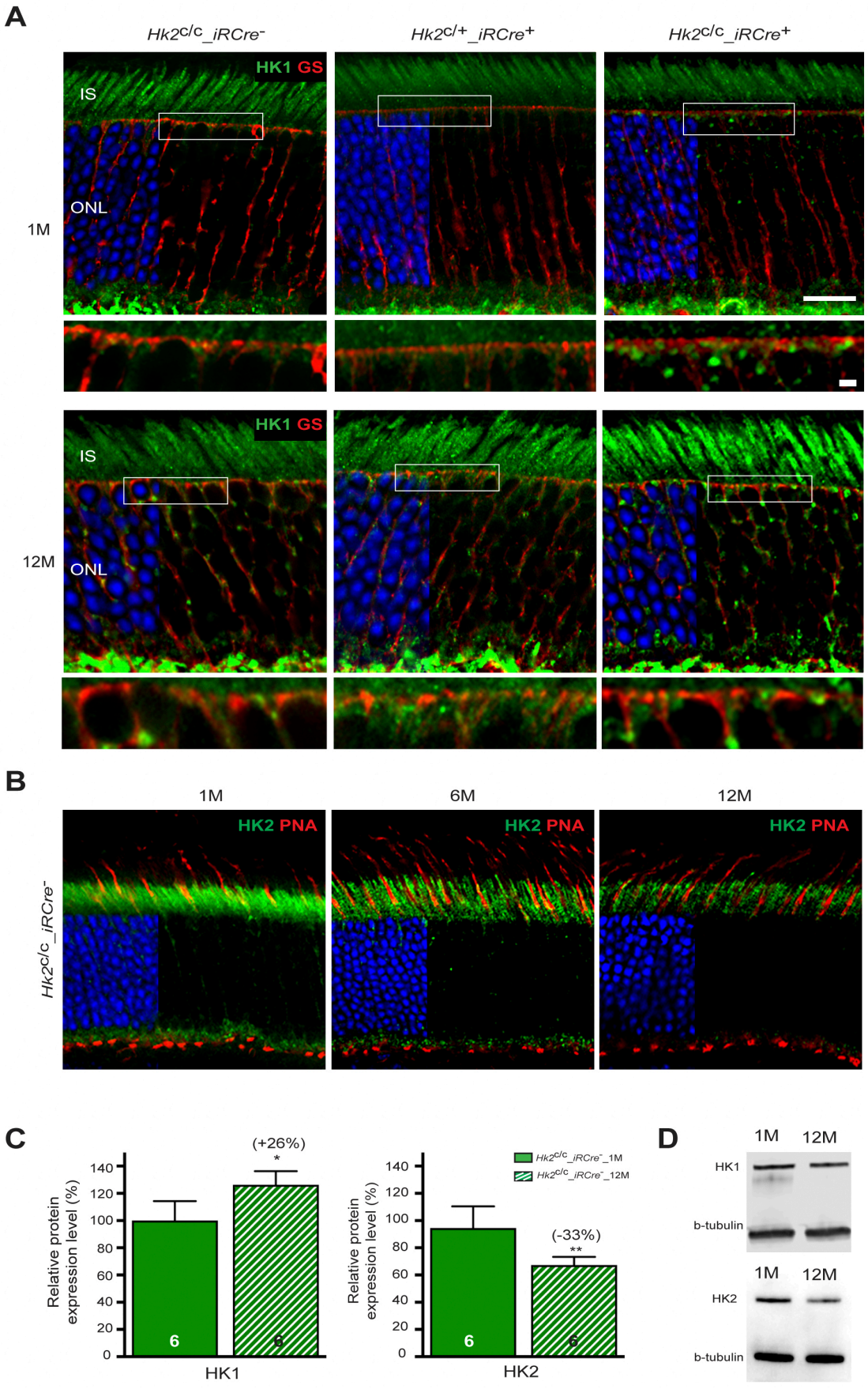
A
Hk2c/c_iRCre-
Hk2c/+_iRCre+
Hk2c/c_iRCre+
HK1 GS
IS
ONL
1M
12M
B
1M
6M
12M
HK2 PNA
Hk2c/c_iRCre-
C
Relative protein expression level (%)
(+26%)
*
HK1
(-33%)
**
HK2
Hk2c/c_iRCre-_1M
Hk2c/c_iRCre-_12M
6
D
1M
12M
HK1
b-tubulin
HK2

Figure S4. **Analysis of HK1 and HK2 expression over time, Related to Figure 5.**
(A) Retinal cross sections stained for glutamine synthetase (GS, red) and HK1 (green) showing no colocalization of large green dots with GS. Higher magnifications of boxed areas are shown in panels below. The number of $HK1^{+}$ dots increases with age in Cre^{-} (wild-type) retinas. DAPI (blue) signal is removed from 60% of panels to visualize red and green signals. IS: inner segments; ONL: outer nuclear layer. Scale bar: 25μm in upper panel and 5μm in lower panel.
(B) Retinal cross sections of $Hk2^{c/c}\_iRCre^{-}$ mice at age indicated showing decreased HK2 expression (green) in PRs with age. Red: PNA; blue: DAPI signal is removed from 60% of panels to visualize red and green signals.
(C, D) HK1 and HK2 quantification determined by western-blot on total retinal extracts at 1 and 12 months of age. Beta-tubulin was used as an internal control. Results are expressed as % change from 1 month-old animals; error bars: ± SD; numbers in bars: number of biological samples (each consisting of 2 retinas from one mouse). With age, HK1 levels increase whereas HK2 levels decrease.

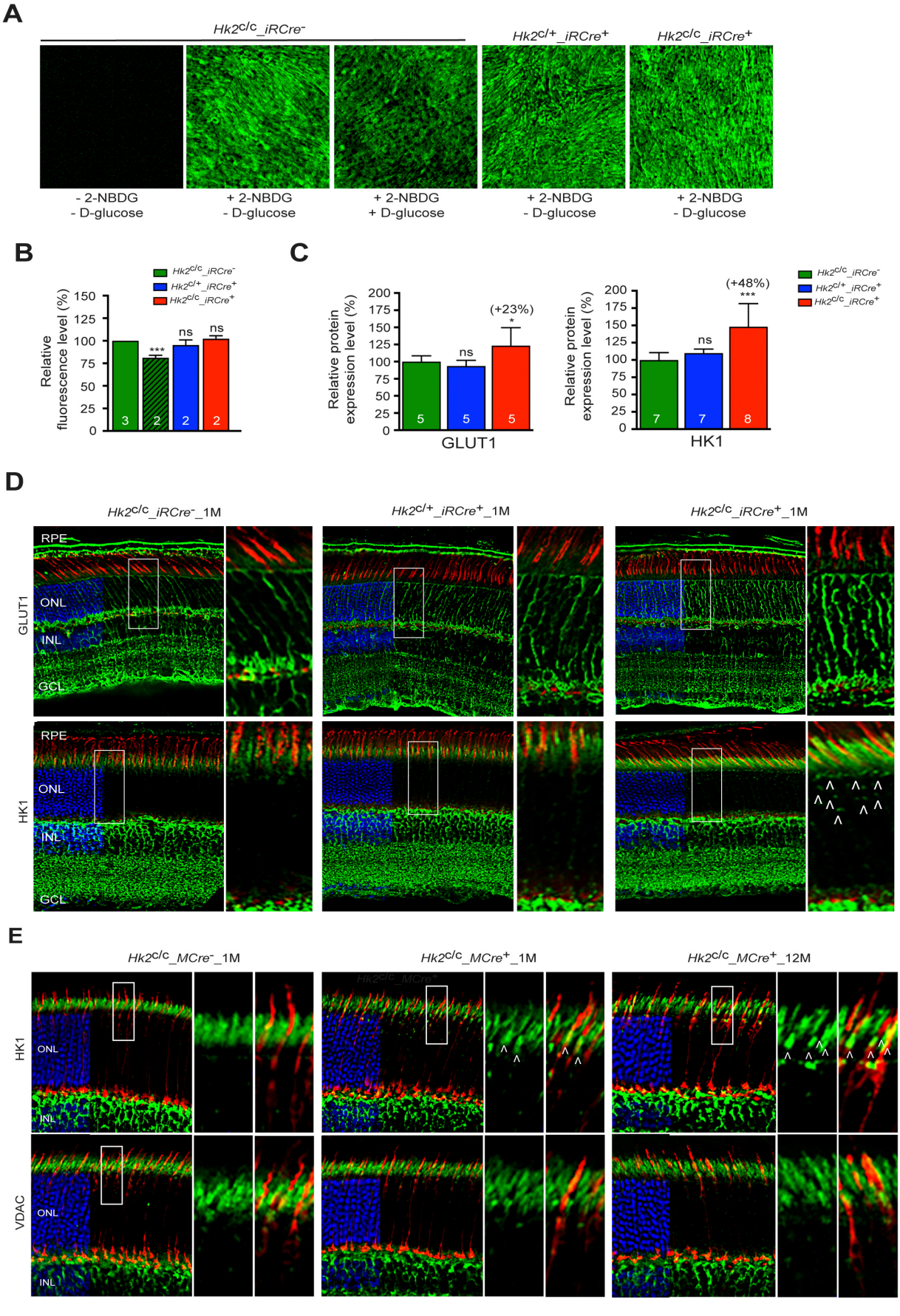
A
Hk2c/c_iRCre-
Hk2c/+_iRCre+
Hk2c/c_iRCre+
- 2-NBDG
- D-glucose
+ 2-NBDG
- D-glucose
+ 2-NBDG
+ D-glucose
+ 2-NBDG
- D-glucose
+ 2-NBDG
- D-glucose
B
Relative fluorescence level (%)
150
125
100
75
50
25
0
***
ns
ns
3
2
2
2
C
Relative protein expression level (%)
200
175
150
125
100
75
50
25
0
(+23%)
*
ns
5
5
5
GLUT1
(+48%)
***
ns
7
7
8
HK1
D
Hk2c/c_iRCre-_1M
Hk2c/+_iRCre+_1M
Hk2c/c_iRCre+_1M
GLUT1
HK1
RPE
ONL
INL
GCL
E
Hk2c/c_MCre-_1M
Hk2c/c_MCre+_1M
Hk2c/c_MCre+_12M
HK1
VDAC
ONL
INL

Figure S5. Glucose uptake is maintained upon loss of HK2, Related to Figure 5.
(A-B) Glucose uptake in PRs measured by incubation of retinal explants with the glucose analogue 2-NBDG followed by (A) microscopy imaging (green signal) and (B) quantification of fluorescence intensity at the level of PR segments. Error bars: ± SD; numbers in bars: number of retinal analyzed.
(C) Quantitative western-blot analysis for GLUT1 and HK1 expression from total retinal lysates of 1-month-old animals. Beta tubulin served as loading control. Levels are expressed as % of wild-type levels. Error bars: ± SD; numbers in bars: number of biological samples (each consisting of 2 retinas from one mouse).
(D, E) Representative images of IHC for proteins indicated to the left of each panel (green signal) on retinal sections of 1-month-old mice (genotypes indicated above each panel). Cones (red signal) were detected by PNA. Blue: DAPI, removed from 60% of panels to visualize red and green signals. Higher magnification of boxed areas is shown to the right of each panel. HK2-depleted rods show significantly enhanced GLUT1 and HK1 (arrowheads) expression, correlating with no change in glucose uptake. HK2-depleted cones also over-expressed HK1 but without changes in the mitochondrial marker VDAC. INL: inner nuclear layer; GCL: ganglion cell layer; ONL: outer nuclear layer; RPE: retinal pigment epithelium.

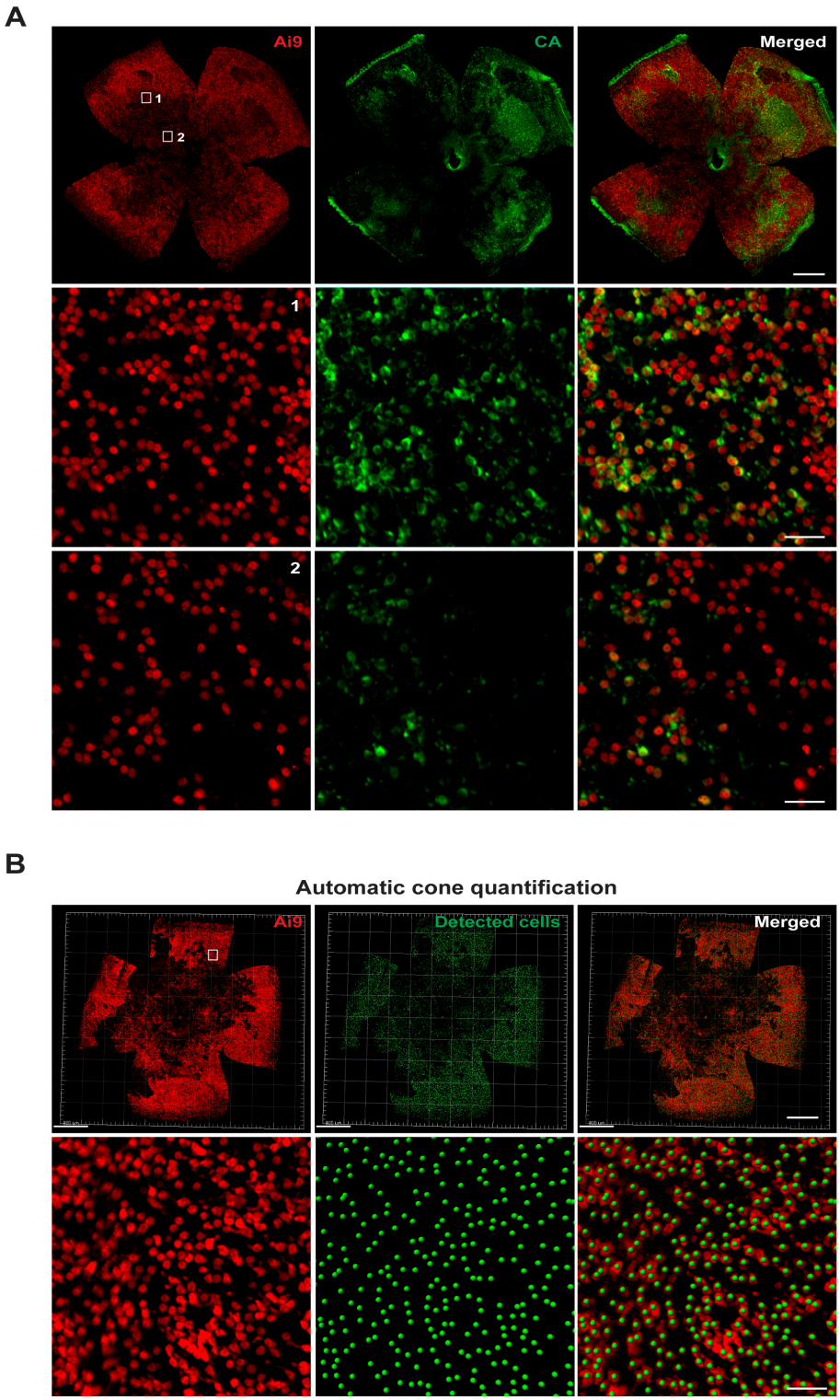

Figure S6. Cone survival analysis, Related to Figure 7
(A) Tiled retinal flat mounts of *rd1_Ai9_MCre*$^{+}$ mice at 2 months of age. Higher magnifications show difference between the Ai9 Cre reporter (red signal) and cone arrestin (green signal) expression during retinal degeneration. (B) Examples of tiled retinal flat mount used for cone survival quantification at 2 months of age in *rd1_Ai9_MCre*$^{+}$ mice. Total cone quantification was performed using Imaris by automatic detection (green dots) of td-Tomato-positive cells (red signal).

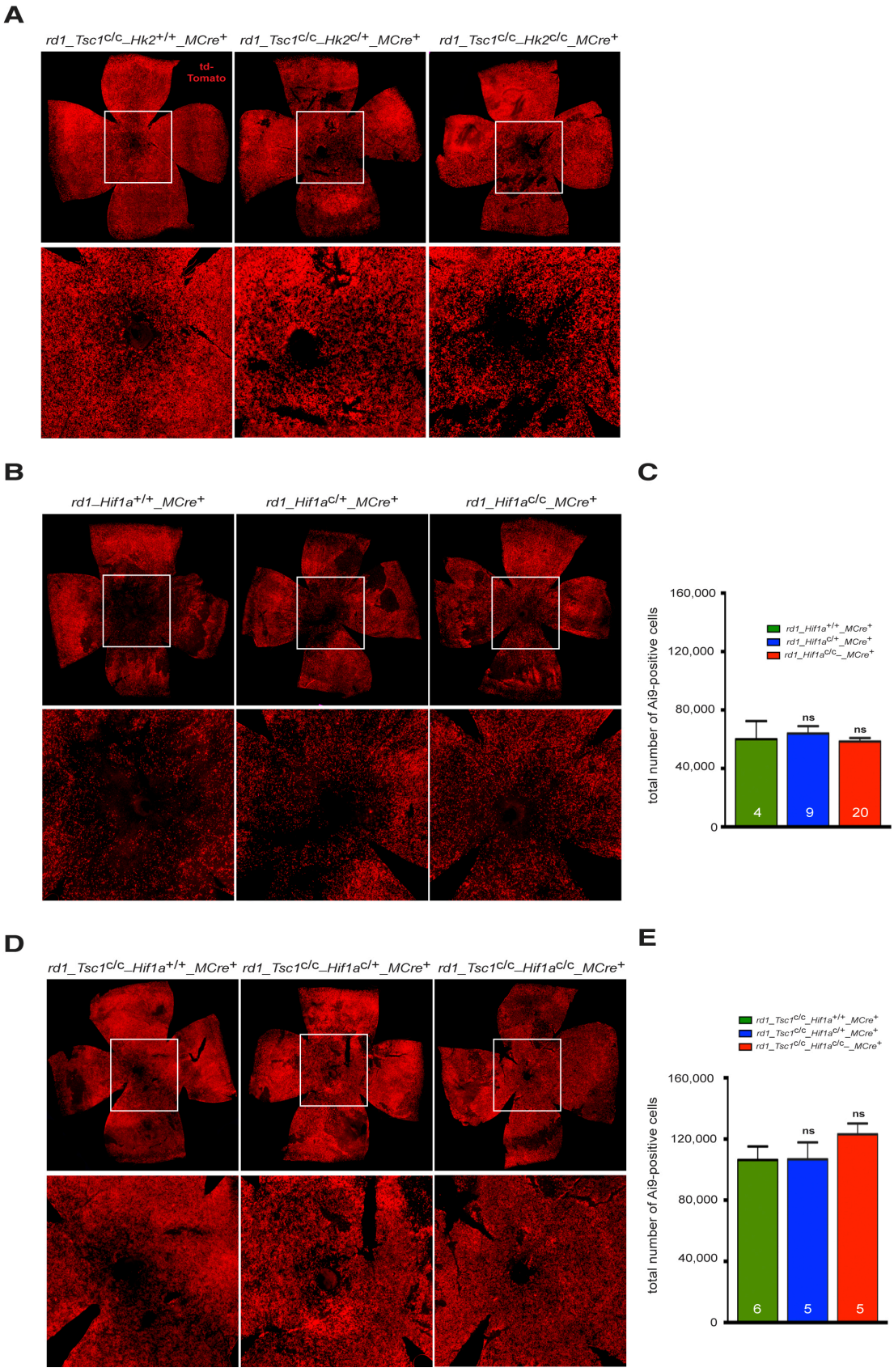
A
rd1_Tsc1c/c_Hk2+/+_MCre+
rd1_Tsc1c/c_Hk2c/+_MCre+
rd1_Tsc1c/c_Hk2c/c_MCre+
td-Tomato
B
rd1_Hif1a+/+_MCre+
rd1_Hif1ac/+_MCre+
rd1_Hif1ac/c_MCre+
C
total number of Ai9-positive cells
160,000
120,000
80,000
40,000
0
rd1_Hif1a+/+_MCre+
rd1_Hif1ac/+_MCre+
rd1_Hif1ac/c_MCre+
ns
ns
4
9
20
D
rd1_Tsc1c/c_Hif1a+/+_MCre+
rd1_Tsc1c/c_Hif1ac/+_MCre+
rd1_Tsc1c/c_Hif1ac/c_MCre+
E
rd1_Tsc1c/c_Hif1a+/+_MCre+
rd1_Tsc1c/c_Hif1ac/+_MCre+
rd1_Tsc1c/c_Hif1ac/c_MCre+
total number of Ai9-positive cells
160,000
120,000
80,000
40,000
0
ns
ns
6
5
5

Figure S7. HK2, but not HIF-1a is required for the survival of *rd1* cones, Related to Figure 7.
(A, B, D) Representative retinal flat mounts of *rd1* mice harboring the indicated conditional alleles at 2 months of age showing less central *Ai9*$^{+}$ cones upon loss of HK2 in cones (A) (red signal indicates td-Tomato) or no changes in cone survival upon loss of HIF-1a in cones (B, D) (higher magnification of boxed area is shown below each panel).
(C, E) Quantification of the total number of td-Tomato-positive cones per retina upon loss of HIF-1a in cones. Errors bars: ± SD; numbers in bars: number of retinas analyzed.

Supplemental Experimental Procedures

Animals

Ai9 Cre reporter (Madisen et al., 2010), *Pde6β*$^{rd1/rd1}$ (Bowes et al., 1990) (here referred as *rd1*), C57BL/6J, *Hif1a*$^{c/c}$ (Ryan et al., 2000) and *Tsc1*$^{c/c}$ (Meikle et al., 2005) mice were purchased from Jackson Laboratories. The *Nrl*$^{-/-}$ (Mears et al., 2001) mice were provided Dr. Hemant Khanna (UMASS Medical School, Worcester, USA). The M-opsin-*Cre* mice (cone-specific Cre line, here referred as M*Cre*) (Le et al., 2004), the iCre79-*Cre* (rod-specific Cre line, here referred as iR*Cre*) (Li et al., 2005), and the *Hk2*$^{c/c}$ mice (Patra et al., 2013) were kindly provided by Dr. Yun Z. Le (University of Oklahoma Health Sciences Center), Dr. Ching-Kang Chen (Baylor College of Medicine) and Dr. Nassim Hay (University of Illinois at Chicago) respectively. To characterize CRE expression in *iRCre*$^{+}$ and *MCre*$^{+}$ mice, *iRCre*$^{+}$ and *MCre*$^{+}$ mice were crossed with the floxed tdTomato reporter line Ai9, resulting in *iRCre*$^{+}$*_Ai9*$^{+}$ mice and *MCre*$^{+}$*_Ai9*$^{+}$ mice. To dissect the role of HK2 in normal rods and cones, the conditional *Hk2* knockout mice were crossed with the *iRCre* line or with the *MCre* line respectively resulting in the *Hk2*$^{c/c}$*_iRCre*$^{-}$, *Hk2*$^{c/+}$*_iRCre*$^{+}$, *Hk2*$^{c/c}$*_iRCre*$^{+}$ or the *HK2*$^{c/c}$_M*Cre*$^{-}$, *Hk2*$^{c/+}$_M*Cre*$^{+}$, *HK2*$^{c/c}$_M*Cre*$^{+}$ littermates that were used for the analyses. To characterize the role of HK2 in metabolically stressed cones, *rd1* and *rd1_Tsc1*$^{c/c}$, mice were first crossed with the *H2*$^{c/c}$ mice. To visualize cones, *rd1_Hk2* and *rd1_Tsc1_Hk2* mice were further crossed with the *MCre*$^{+}$*_Ai9*$^{+}$ mice. A similar crossing approach was used to evaluate the role of HIF-1a in metabolically stressed cones. Here only males were used for analysis. All animals were kept on a 12 hours day/night cyle with constant light conditions ranging from 10-15 lux with unrestricted access to food and water. All experiments and procedures were approved by the Institutional Animal Care and Use Committee (IACUC) of the University of Massachusetts Medical School.

Electroretinography (ERG)

Retinal function of *Hk2_iRCre* and *Hk2_MCre* mice was evaluated using bilateral full-field flash ERG as previously described (Ma et al., 2015). Initial ERG measurements were recorded at 1 month of age and every subsequent 1-2 months up to 18 months of age, the latest time point evaluated in this study. The dark-adapted animals were anesthetized with ketamine (100mg/kg) and xylazine (10mg/kg) and pupils were fully dilated by topical administration of 2.5% Phenylephrine and 1% Tropicamide. Body temperature was maintained at 37C using a heating pad during the entire procedure. The Espion3 console in conjunction with the ColorDome (Diagnosys LLC, Lowell, MA, USA) and gold-wired electrodes placed on the corneas were used. ERG responses were recorded in a standardized fashion according to the International Society for Clinical Electrophysiology of Vision (ISCEV) recommendations, using a protocol described previously (Ma et al., 2015).

The peak times and the amplitudes of the ERG responses were measured according to the standard practice. The amplitude of the a-wave was measured from the baseline to trough and at different fixed time points after flash onset. The amplitude of the b-wave was measured from the trough of the a-wave to the peak of the b-wave. Peak times were measured from flash onset. Analysis of the leading edge of the a-wave of rod responses (generated in response to a flash of 10 cd s/m^2) was performed according to the method previously described by Hood and Birch (Hood and Birch, 1996). The records were normalized to have the same or maximal amplitude at about 23ms (trough in iR*Cre*$^{-}$). A change in sensitivity was defined as a change that acts as if the flash intensity was decreased. A change in the maximum response was defined as a change that scales the entire leading edge by the same factor. Changes in S have been attributed to changes in one or more of the steps of phototransduction, such that the amplification/speed of phototransduction is affected; but also to a decrease in the density of rhodopsin in individual discs and/or shortened outer segments. A change in the maximal response was hypothesized to be caused by changes in the polarization of the membrane by the steady field and/or by changes in the recycling of glutamate vesicles at the synaptic connection (Hood and Birch, 1996).

Fundoscopy

Fundus photography was performed bilaterally on *Hk2_iRCre* mice at 18 months of age as previously described (Ma et al., 2015; Venkatesh et al., 2013). Before clinical examinations, the pupils were dilated and animals anesthetized as described above. Fundus photographs were taken with a Micron III retinal camera connected to a digital imaging system.

Quantification of Cre-positive cells using flow cytometry

Retinas from 2 *Ai9*$^{+/+}$*_MCre*$^{+}$ mice and 2 *Ai9*$^{+/+}$*_iRCre*$^{+}$ mice were isolated, pooled and dissociated to single cells by digestion with papain. Briefly, before dissociation, 10μL papain (Worthington, 39.6mg/ml, 30U per mg protein) was activated with 10μL cysteine/EDTA mix (pH 8.0, 25mM cysteine, 5mM EDTA) in 380μL Hanks' balanced salt solution (HBSS) for 15min at 37C. Retinas were dissected in cold HBSS and incubated in the activated papain solution for 5-8min at 37C. 800μL DMEM containing 5% fetal bovine serum was added to the cell suspension and the solution

gently triturated 10 times with a pipette to further dissociate the cells. The cell suspension was filtered into a 5-mL polypropylene round-bottom Falcon tube and maintained on ice. Cells positive for td-Tomato were quantified using flow cytometry.

Immunohistochemistry on retinal cross-sections and 3D-deconvolution

Immunohistochemistry labeling was performed on 20μm retinal cryo-sections as described previously (Venkatesh et al., 2013). The following primary antibodies and concentrations were used: rabbit α-cone arrestin (1:500; Millipore #MAB15282), mouse monoclonal α-cone arrestin (produced in the Punzo laboratory), rabbit α-GLUT1 (1:300; Alpha Diagnostics #GT11-A), mouse α-GS (1:300; Millipore #MAB302), rabbit α-HK1 (1:300; Cell Signaling #2024), rabbit α-HK2 (1:300; Cell Signaling #2867), rabbit α-LDHA (1:500; Sigma-Aldrich #AV54777), rabbit α-LDHB (1:500; Sigma-Aldrich #SAB2108609), rabbit α-LM opsin (1:500; Millipore #MAB5405), goat α-S opsin (1:500; SantaCruz #sc16363), rabbit α-PKM2 (1:500; Cell Signaling #4053), rabbit α-VDAC (1:500; Cell Signaling #4661), and rhodamine- or fluorescein-labeled peanut aggulutinin lectin (PNA) (1:500; Vector Laboratories #FL-1071 or #RL-1072). All secondary antibodies (donkey, diluted 1:500) were purchased from Jackson ImmunoResearch and were purified $F(ab)_2$ fragments that displayed minimal cross-reactivity with other species. Nuclei were counterstained with DAPI. All images were acquired with the Leica DM5500 fluorescent microscope equipped with a motorized stage, for tiling and z-stack image acquisition and deconvolution software for confocal-like image quality. At least 3 eyes from different mice were used for histological analysis of each mouse line.

Quantification of rod survival on retinal sections

Quantification of rod survival was performed in two ways. First, we measured the thickness of the ONL from 3-5 consecutive sections per eye, as previously described (Zieger and Punzo, 2016). All sections were through the optic nerve in the ventral-dorsal axis. ONL thickness was measured 3 times per section at 10 inferior and 10 superior position spaced 200μm apart. An average was generated for each section and for each retina. The measurements were taken in DAPI-stained sections. Second, the total number of ONL nuclei on the same sections was automatically quantified across one focal plan of using Imaris Software, as previously described (Petit et al., 2017). An average was generated for each sample.

Quantification of cone survival on retinal flat-mounts

We used an automatic method for quantifying cones over the entire retinal surface, rather than counting the number of cones in a few individual fields because in *rd1* mice, cone degeneration is patchy and progresses from the center to the periphery. Quantifying the total number of cones is independent of the degeneration pattern and the orientation of the retina. Antibody staining was performed as described above. Retinal flat-mount images were acquired by tiling individual images (Leica DM55000) over the entire retinal surface area with an automated scanning stage. $Ai9^+$, PNA^+, LM $opsin^+$ or S $opsin^+$ cones were quantified using the automatic cell-counting feature (Spots) in Imaris software.

Transmission Electron Microscopy

Electron microscopy was carried out as previously described (Ma et al., 2015). At least 3 eyes from different mice were used for analysis of each mouse line. Briefly, mouse eyes were enucleated and fixed in 2.5% glutaraldehyde in 0.1M sodium cacodylate buffer (pH 7.2) for 20min at room temperature. Subsequently, cornea and lens were removed and eyecups were fixed overnight at 4C in the same fixative. Eyecups were postfixed in 1% osmium tetroxide in cacodylate buffer, dehydrated in graded ethanol solutions and embedded in epoxy resin. Serial ultrathin sections (70nm) were cut with an ultra-microtome (Leica Reichart-Junch; Leica Microsystems), collected onto formvar-coated copper grids, stained with uranyl acetate and lead citrate and examined using a Philips CM-10 transmission electron microscope (Philips, Eindhoven, The Netherlands). OS length was measured at multiple locations on semi-thins radial sections of embedded eyes. An average was generated for each retina. Bright field images were acquired with the Leica DM5500. For the quantification of mitochondria, random electron microscopy images of the ONL were taken at x2600 and x4600. The number of mitochondria per cell was calculated by counting the total number of mitochondria reported to the total number of cell nuclei in each image. At least 200 cell nuclei were counted in per individual mouse.

Quantitative Western-blots

For analysis of HK2 expression during retinal development, four retinas from 3 different animals of each time-point were pooled. For analysis of changes in metabolic gene expression, two retinas from 1 animal were pooled and considered as one biological sample. Five to eight biological samples for each mouse line were analyzed. Protein extracts from adult C57/Bl6 liver and HEK293 cells were always used as negative or positive control for the expression of HK2, respectively. Tissues and cells extracts were prepared as previously described (Petit et al., 2012) or (Venkatesh et al., 2015). Protein lysates were separated on a 4-15% Tris-Glycine gradient gel (Biorad) followed by electrotransfer

onto a nitrocellulose membrane. For GLUT1, LDHB and HK2 western-blots, membranes were blocked in 5% fat-free milk and incubated overnight at 4C with primary antibodies: rabbit α-GLUT1 (1:1000; Alpha Diagnostics #GT11-A), rabbit α-LDHB (1:1000; Sigma-Aldrich #SAB2108609) and rabbit α-HK2 (1:1000; Cell Signaling #2867). After washing, incubation with HRP-conjugated secondary antibodies (1:10,000, Santa-Cruz Biotechnology) was performed. All antibody incubations were performed in the presence of 0.1% Tween-20 and 5% fat-free milk. Immuno-reactive bands were visualized using SuperSignal West Femto detection reagents (ThernoScientific) and quantified with the Chemidoc Touch Imaging System (Biorad). For the other western-blot results, instead of fat-free milk powder, Odyssey Blocking Buffer (LICOR #927-40000) was used for blocking and antibody incubations using: rabbit α-HK1 (1:1000; Cell Signaling #2024), rabbit α-HK2 (1:1000; Cell Signaling #2867), rabbit α-LDHA (1:1000; Sigma-Aldrich #AV54777), rabbit α-PKM2 (1:2000; Cell Signaling #4053), rabbit α-VDAC (1:1000; Cell Signaling #4661), total OXPHOS rodent western-blot antibody cocktail (1:250; Abcam #ab110413), rabbit α-beta tubulin (1:1000; Cell Signaling #2146) and mouse α-beta tubulin (1:2000; Sigma-Aldrich #8328). No detergent was added during blocking. Secondary antibodies were infrared dye-conjugated (1:10,000; LI-COR). Membranes were scanned on an Odyssey Infrared Scanner from LI-COR to detect and quantify signal. Images were exported as black and white. Average result from all Cre- animals was set as 100%.

RT-qPCR

Two retinas of one animal were pooled to isolate RNA and considered as one biological sample. Two to three biological samples for each mouse line were analyzed. Total RNA was isolated using TRIzol Reagent (Invitrogen Life Technologies). Rnase-free DNase I (Ambion DNA-free kit; Invitrogen Life Technologies) was used according to the manufacturer's instructions to remove contaminating DNA before generation of cDNA by reverse-transcription. One microgram of total RNA was reverse-transcribed using random hexamer primers and Transcriptase High Fidelity (Roche) as per the manufacturer's instructions. Control assays without addition of reverse transcriptase were included and the products were used in the subsequent RT-qPCR as negative controls. For each RNA preparation, RT and negative controls were performed in duplicate. RT-qPCR was performed using standard protocol of the Bio-Rad CFX96 Real-Time System. Briefly, 2μL of a 1/20 dilution of cDNA was added to 10μL of the 2x SYBR green PCR master mix (Kapa Biosystems) containing 0.8μM primers. Each reaction was performed in triplicate and the data were normalized to GAPDH (also calculated from triplicate reactions) using the 2-ddCt method. The following primers were used: *β-actin* (5'-ACTGGGACGACATGGAGAAG-3' and 5'-GGGGTGTTGAAGGTCTCAAA-3'), *Gapdh* (5'-TGCACCACCAACTGCTTAGC-3' and 5'-GGCATGGACTGTGGTCATGAG-3') and *Hk2* (5'-GGAACCCAGCGTTTGACCA-3' and 5'CAGGGGAACGAGAAGGTGAAA-3').

Glucose uptake assay

Retinas were dissected in cold DMEM. Retinal explants were stained with fluorescent D-glucose analogue 2-[H-(7-nitrobenz-2-oxa-1,3-diazol-4-yl) amino]-2-deoxy-D-glucose (2-NBDG, 1uM in water) in DMEM medium with or without D-glucose for 45 min at 37C. Retinal explants were then washed four times with ice-cold PBS-1X and DAPI mix to remove excess 2-NBDG. Retinas were then flat-mounted between two pre-chilled slide covers and analyzed under fluorescent microscope within <10min. Images were taken at the level of PR segments at 5 different locations/retina. Fluorescent measurements were made in duplicate, in two different experiments using the Leica Application Suite LAS.

Lactate and NADPH assay

Secreted lactate was evaluated with the Lactate assay kit from Eton Bioscience. NADP and NADPH were quantified using Fluoro NADP/NADPH kit from Cell Technology. Both assays were performed in triplicate using 2-3 biological samples, with each biological sample consisting of 2 retinas. Retinas were dissected in cold DMEM media, rinsed in PBS, sonicated in assay buffer and processed following manufacturer's instructions. Results were normalized per retina.

Supplemental References

Bowes, C., Li, T., Danciger, M., Baxter, L.C., Applebury, M.L., and Farber, D.B. (1990). Retinal degeneration in the rd mouse is caused by a defect in the beta subunit of rod cGMP-phosphodiesterase. Nature *347*, 677-680.

Feodorova, Y., Koch, M., Bultman, S., Michalakis, S., and Solovei, I. (2015). Quick and reliable method for retina dissociation and separation of rod photoreceptor perikarya from adult mice. MethodsX *2*, 39-46.

Hood, D.C., and Birch, D.G. (1996). Assessing abnormal rod photoreceptor activity with the a-wave of the electroretinogram: applications and methods. Doc Ophthalmol *92*, 253-267.

Le, Y.Z., Ash, J.D., Al-Ubaidi, M.R., Chen, Y., Ma, J.X., and Anderson, R.E. (2004). Targeted expression of Cre recombinase to cone photoreceptors in transgenic mice. Mol Vis *10*, 1011-1018.

Li, S., Chen, D., Sauve, Y., McCandless, J., Chen, Y.J., and Chen, C.K. (2005). Rhodopsin-iCre transgenic mouse line for Cre-mediated rod-specific gene targeting. Genesis *41*, 73-80.

Ma, S., Venkatesh, A., Langellotto, F., Le, Y.Z., Hall, M.N., Ruegg, M.A., and Punzo, C. (2015). Loss of mTOR signaling affects cone function, cone structure and expression of cone specific proteins without affecting cone survival. Exp Eye Res *135*, 1-13.

Madisen, L., Zwingman, T.A., Sunkin, S.M., Oh, S.W., Zariwala, H.A., Gu, H., Ng, L.L., Palmiter, R.D., Hawrylycz, M.J., Jones, A.R.*, et al.* (2010). A robust and high-throughput Cre reporting and characterization system for the whole mouse brain. Nat Neurosci *13*, 133-140.

Mears, A.J., Kondo, M., Swain, P.K., Takada, Y., Bush, R.A., Saunders, T.L., Sieving, P.A., and Swaroop, A. (2001). Nrl is required for rod photoreceptor development. Nat Genet *29*, 447-452.

Meikle, L., McMullen, J.R., Sherwood, M.C., Lader, A.S., Walker, V., Chan, J.A., and Kwiatkowski, D.J. (2005). A mouse model of cardiac rhabdomyoma generated by loss of Tsc1 in ventricular myocytes. Hum Mol Genet *14*, 429-435.

Patra, K.C., Wang, Q., Bhaskar, P.T., Miller, L., Wang, Z., Wheaton, W., Chandel, N., Laakso, M., Muller, W.J., Allen, E.L.*, et al.* (2013). Hexokinase 2 is required for tumor initiation and maintenance and its systemic deletion is therapeutic in mouse models of cancer. Cancer Cell *24*, 213-228.

Petit, L., Lheriteau, E., Weber, M., Le Meur, G., Deschamps, J.Y., Provost, N., Mendes-Madeira, A., Libeau, L., Guihal, C., Colle, M.A.*, et al.* (2012). Restoration of vision in the pde6beta-deficient dog, a large animal model of rod-cone dystrophy. Mol Ther *20*, 2019-2030.

Petit, L., Ma, S., Cheng, S.Y., Gao, G., and Punzo, C. (2017). Rod Outer Segment Development Influences AAV-Mediated Photoreceptor Transduction After Subretinal Injection. Hum Gene Ther *28*, 464-481.

Ryan, H.E., Poloni, M., McNulty, W., Elson, D., Gassmann, M., Arbeit, J.M., and Johnson, R.S. (2000). Hypoxia-inducible factor-1alpha is a positive factor in solid tumor growth. Cancer Res *60*, 4010-4015.

Venkatesh, A., Ma, S., Langellotto, F., Gao, G., and Punzo, C. (2013). Retinal gene delivery by rAAV and DNA electroporation. Curr Protoc Microbiol *Chapter 14*, Unit 14D 14.

Venkatesh, A., Ma, S., Le, Y.Z., Hall, M.N., Ruegg, M.A., and Punzo, C. (2015). Activated mTORC1 promotes long-term cone survival in retinitis pigmentosa mice. J Clin Invest *125*, 1446-1458.

Zieger, M., and Punzo, C. (2016). Improved cell metabolism prolongs photoreceptor survival upon retinal-pigmented epithelium loss in the sodium iodate induced model of geographic atrophy. Oncotarget *7*, 9620-9633.